Title: Regulation of a surface chlorophyll hotspot by wind-driven upwelling and eddy circulation in the Santa Barbara Channel, Southern California

Authors: Rachel D. Simons[1*] and Dylan Catlett[2]

[1*] Earth Research Institute, University of California, Santa Barbara, CA, USA

[2] Woods Hole Oceanographic Institution, Wood Hole, MA, USA

[*] Corresponding Author. Address: Email address: simons@eri.ucsb.edu

Keywords: upwelling, eddies, chlorophyll, phytoplankton, ROMS, nitrogen

Abstract

While most of the U.S. Pacific coast is dominated by strong wind-driven upwelling in the spring and regular seasonal cycles of phytoplankton primary production, the Southern California Bight has weak intermittent wind-driven upwelling and low phytoplankton concentrations due to its irregular sheltered coastline. However, the Santa Barbara Channel (SBC), located in the northern Southern California Bight, contains an anomalous hotspot of phytoplankton biomass. We use 3D ocean circulation and particle tracking models, an empirical temperature-nitrate relationship, and satellite observations of surface chlorophyll from 1998 to 2007 to determine how wind-driven upwelling and cyclonic eddy circulation govern phytoplankton dynamics in the SBC. Our findings show that elevated surface chlorophyll in the spring is driven by the coupling of wind-driven upwelling and cyclonic eddy circulation and requires the presence of both high nitrate from wind-driven upwelling and prolonged residence times from eddy circulation. Long residence times, created by persistent cyclonic eddy circulation, allow nitrate transported into the surface layer by wind-driven upwelling to be retained in the SBC long enough to meet the required timescales for phytoplankton nutrient uptake and accumulation, overcoming the typically weak wind-driven upwelling of the Southern California Bight. Typical spring upwelling periods (SUPs) have high levels of surface chlorophyll, which are produced by the balanced coupling of upwelling strength and cyclonic eddy circulation. For two years of our study, 1998 and 1999, the SUP did not correlate with elevated surface chlorophyll. Corresponding to a strong El Niño event, the 1998 SUP had exceptionally weak wind-driven upwelling, which did not produce sufficient levels of nitrate to stimulate elevated surface chlorophyll. For the 1999 SUP, a strong La Niña event produced unusually strong wind-driven upwelling, which resulted in very high levels of nitrate, but suppressed eddy circulation and residence times to the point where phytoplankton biomass could not accumulate in the SBC. These anomalous SUPs illustrate that when wind-driven upwelling is too strong or weak, the balance between wind-driven upwelling and cyclonic eddy circulation is disrupted, resulting in a dramatic reduction of

surface chlorophyll, which may become more frequent with climate-driven upwelling changes in the future.

1.0 Introduction

While continental margins contain only a fraction of the world's oceans, they have been estimated to produce 10-15% of the global primary production (Thunell et al. 2007; Fennel and Wilkin 2009; Levin et al. 2015). Eastern boundary upwelling systems (EBUSs), which include the California EBUS, are among the most productive continental margin ecosystems in the world and are of particular concern as they are being increasingly impacted from climate change, the harvesting of marine resources, and coastal development (Levin et al. 2015). Encompassing the west coast of the United States, the California EBUS is one of the largest EBUSs in the world and is defined by a seasonal cycle of primary production. Wind-driven upwelling in the California EBUS is strongest in the spring and early summer when alongshore winds drive offshore Ekman transport and nutrients are vertically transported into the surface layer stimulating primary production (Legaard and Thomas 2006; Henson and Thomas 2007; García-Reyes and Largier 2012). Messie and Chavez (2015) found that in addition to nutrient supply, physical export of nutrients is an important regulator of primary production in the California EBUS. Physical export can limit primary production if nutrients introduced to the surface layer are transported off the shelf before uptake by phytoplankton can occur. Thus, to understand the variability of primary production in EBUSs, the physical processes that retain nutrients in the surface layer on the shelf need to be understood (Lachkar and Gruber 2011; Messié and Chavez 2015).

Located in the southern region of the California EBUS is the Southern California Bight (SC Bight, Fig. 1), which encompasses the southern California coast and the eight Channel Islands. While most of the California EBUS is dominated by strong spring upwelling and regular seasonal cycles of primary production, the SC Bight has weak, intermittent upwelling due to its irregular, sheltered coastline, which results in low levels of primary production year round (Winant and Dorman 1997; Dorman and Winant 2000). However, the Santa Barbara Channel (SBC), located within the northern SC Bight, regularly contains anomalously high phytoplankton biomass and primary productivity compared to the rest of the SC Bight (Fig. 1, Mantyla et al. 1995; Henderikx Freitas et al. 2017; Santora et al. 2017). Due in part to this unusually productive environment, the SBC supports a uniquely biodiverse ecosystem of extensive kelp forests, intertidal habitats, and sandy beaches along with large populations of seabirds, marine mammals, fishes, and plankton (Beers et al. 1986; Fiedler et al. 1998; Miller et al. 2011; Dugan and Hubbard 2016).

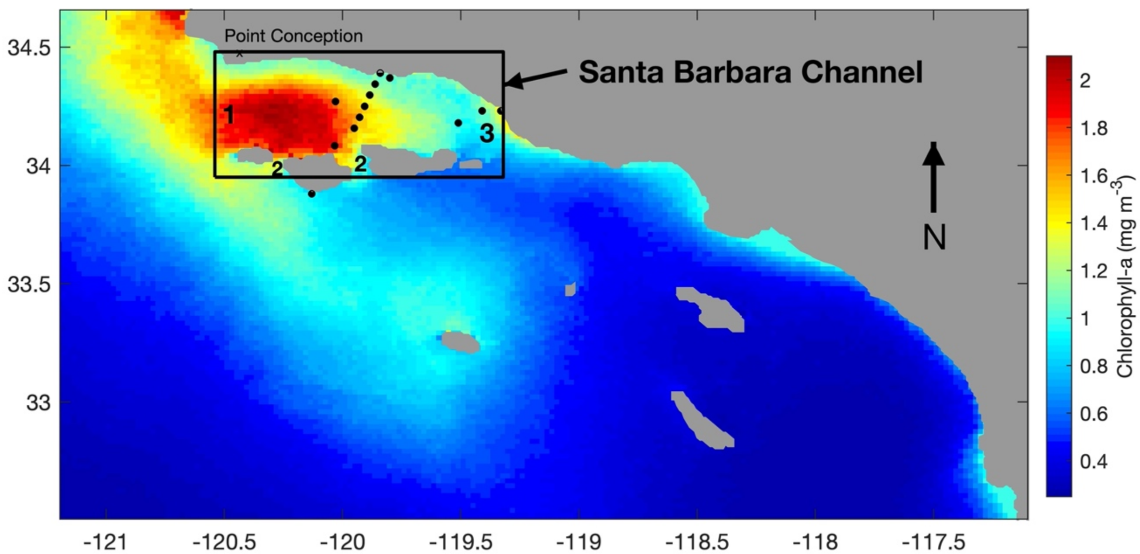

Figure 1: Mean surface chlorophyll-a concentrations (mg m^{-3}) in the Southern California Bight from satellite data (Kahru et al. 2012, 2015, http://spg-satdata.ucsd.edu). Location of the Santa Barbara Channel (SBC) is identified by the black box. SBC boundaries are identified as 1-West, 2-South, and 3-East. The solid black circles show the sample locations of the CalCOFI and UCSB Plumes and Blooms programs.

The SBC is a 50 km wide, 100 km long, and 500 m deep basin, which is bounded to the north by the Southern California coast and the south by the Northern Channel Islands (Fig. 1). To the north of the SBC, the oceanographic regime is characterized by the cold, nutrient-rich waters of the southward flowing California Current (CC), which can extend up to 1,000 km offshore (Hickey 1993; Bray et al. 1999). To the south of the SBC, the oceanographic regime is dominated by the warm, nutrient-poor waters of the northward flowing Southern California

Countercurrent (SCC, Hickey 1993; Bray et al. 1999). The SBC is the transition zone where these two regimes meet, creating a dynamic physical and biological environment.

The two dominant circulation patterns associated with phytoplankton accumulation in the SBC are wind-driven upwelling and cyclonic eddy circulation (Anderson et al. 2006; Brzezinski and Washburn 2011; Matson et al. 2019). For this paper, wind-driven upwelling will be referred to as “upwelling”, and cyclonic eddy circulation as “eddy circulation”. Driven by persistent, steady winds from the west, upwelling occurs along the mainland coast of the SBC and is strongest in the spring and early summer (Winant and Dorman 1997; Harms and Winant 1998; Melton et al. 2009). Upwelling also occurs in the SBC in the late summer and early fall, but is frequently interrupted by wind reversals, which transport warm nutrient poor waters back towards the coastline (Washburn and McPhee-Shaw 2013). McPhee-Shaw et al. (2007) estimated that spring upwelling accounted for 70% ± 15% of the total annual nutrient delivery to the inner-shelf. During spring upwelling, large phytoplankton blooms, covering more than 50% of the SBC, are observed, but smaller blooms can occur at any time during the year (Otero and Siegel 2004; Santoro et al. 2010). Similar to the California EBUS, upwelling intensity in the SBC is affected by the El Niño Southern Oscillation (ENSO) with strong El Niño events suppressing upwelling and strong La Niña events enhancing it (Schwing et al. 2000; Jacox et al. 2018).

Eddy circulation is present periodically throughout the year in the western SBC and ranges in diameter from 5 to 40 km, at times penetrating down to 300 m. Eddy circulation occurs when a poleward pressure gradient balances equatorward wind stress (Harms and Winant 1998; Dever et al. 1998; Oey et al. 2004) and persists for an average of two weeks, ranging from a few days to months depending on ocean conditions (Nishimoto and Washburn 2002; Beckenbach and Washburn 2004). Eddy circulation is also affected by the ENSO. When El Niño conditions cause atypically weak upwelling and wind relaxation, the equatorward wind stress balances the poleward pressure gradient for unusually long periods of time allowing eddy circulation to persist for months. In contrast, La Niña conditions cause unusually strong equatorward wind stress, which dominates the poleward pressure gradient and does not allow stable eddy circulation to form (Nishimoto and Washburn 2002; Simons et al. 2015).

Based on a field study of water column measurements from 16 seasonal channel-wide cruises, Brzezinski and Washburn (2011) found that 80% of the variability in phytoplankton primary production was explained by the presence of upwelling and eddy circulation. Through their work along with Anderson et al. (2006), Krause et al. (2013), and Simons et al. (2015), the following hypotheses were proposed connecting upwelling and eddy circulation to the anomalously high primary production in the SBC. Nutrient-rich water is introduced into the surface layer of the SBC by three processes; (1) upwelling along the mainland coast, (2) advection of upwelled water from the west into the southern SBC by eddy circulation, and (3) eddy circulation through the uplift of isopycnals, also known as eddy pumping (McGillicuddy 2016). After these processes occur, eddy circulation retains nutrient-rich water in the SBC by creating an environment of long residence times, allowing phytoplankton to accumulate.

In this study, we integrate a high-resolution 3D Regional Ocean Modeling System (ROMS) with satellite and field observations to determine the interactive roles of upwelling, eddy circulation, and nutrient transport in regulating mesoscale phytoplankton blooms in the SBC. The ROMS is used to identify the presence and strength of upwelling and eddy circulation in the SBC over a 10-year period from 1998-2007. Driven by the ROMS, a 3D particle tracking model is used to estimate residence time and the source location of water in the SBC. Surface chlorophyll-a concentrations from satellite data are used as a proxy for phytoplankton biomass. We compare mean decadal, annual, and interannual patterns of modeled upwelling, eddy circulation, nutrient availability, source water location, and residence times to surface chlorophyll-a concentrations.

2.0 Methods

2.1 *Ocean circulation modeling and eddy detection*

The 3D ocean circulation model used for this study was a high-resolution Regional Ocean Modeling System (ROMS) applied to the SC Bight (Shchepetkin and McWilliams 2005; Dong and McWilliams 2007; Dong et al. 2009). Our analysis was conducted on 6-hr averaged offline solutions of velocity and temperature from the ROMS for 1998-2007. The model domain, shown in Fig. 1, contains the SC Bight, which includes the SBC. The model grid spans a latitude of $32^{\circ}17'$ N to $34^{\circ}45'$ N and a longitude of $117^{\circ}06'$ W to $121^{\circ}12'$ W with 1 km horizontal resolution and 40 vertical levels. The model has been validated for seasonal, annual, and interannual mesoscale circulation (Dong et al. 2009; Ohlmann and Mitarai 2010) and has successfully reproduced upwelling events in the SC Bight (Dong et al. 2011) and the interannual variability of eddy circulation in the SBC (Simons et al. 2015). As shown in Fig. 1, our study area is the SBC, which spans a latitude of $33^{\circ}57'$ N to $34^{\circ}29'$ N and a longitude of $119^{\circ}20'$ W to $120^{\circ}34'$ W.

Since our goal is to determine how upwelling and eddy circulation regulate surface chlorophyll-a concentrations in the SBC, we focus on the SBC surface layer defined as the top 30 m of the water column. This definition is based on depth measurements of the SBC euphotic zone of 24 m $\pm$ 9.5 m from Brzezinski and Washburn (2011) and observations by Krause et al. (2013), which showed that 30 m is generally near or below the base of the surface layer. Venrick (1998) also observed that chlorophyll in the SBC was consistently concentrated in the upper 25 m of the water column.

Using the ROMS, eddy circulation in the SBC was quantified using an eddy detection algorithm developed by Nencioli et al. (2010). This eddy detection algorithm was developed using vector geometry and identifies the center, shape, lifespan, and trajectory of all eddies in horizontal flow fields. In previous work, this algorithm has been successfully applied to the ROMS solutions used in the study (Nencioli et al. 2010; Dong et al. 2012; Simons et al. 2015) and to field observations of eddies in the South China Sea (Chen et al. 2011; Wang et al. 2021) and the North Pacific Ocean (Liu et al. 2012). For this analysis, the algorithm was applied to horizontal velocity fields from the ROMS solutions that were depth-averaged over the surface layer, the top 30 m of the water column, and provided a dataset of eddy presence, location, size, and lifespan every six-hours for the 10-year modeling period of 1998-2007.

2.2 *Estimating residence time and source water zone with particle tracking*

To estimate the residence time and source location of water in the SBC, a 3D particle tracking model (PTM) was used. Driven by the stored flow fields from the ROMS, the PTM used tri-linear interpolation to identify the velocity of the particles within a grid cell and then moved the particles in time using a fourth-order accurate Adams-Bashforth-Moulton predictor-corrector method (Carr et al. 2008; Mitarai et al. 2009). Particles were released daily throughout the SBC surface layer horizontally on a 1 km^2 grid and vertically every 5 m from 5 m to 30 m below the surface. Particles were tracked passively forward and backwards in time in separate simulations for 60 days, resulting in 54,744 particles released daily and a total of 199.8 million particles tracked for the 10-year modeling period.

The forward particle tracking simulations were used to calculate residence time in the SBC. First, the horizontal location and tracking time for all particles released over the previous 60 days were identified for each day of the 10-year modeling period. Then, the mean tracking time of the particles located within each grid cell (1 km^2) was calculated for all grid cells in the SBC. This method created a 2D distribution of mean tracking times or residence time (RT) for each day of the modeling period where RT represented the mean length of time that particles remained within a grid cell. The residence time within the eddy (RT_{eddy}) was determined using the eddy detection scheme to identify the horizontal area of the eddy and then averaging the RT over the eddy's area.

The reverse particle tracking simulations were used to calculate the percentage of water in the SBC surface layer coming from four different source water zones: West, East, South, and SBC. The source water zone of a particle was defined by the boundary, West, East, or South

(Fig. 1), where the particle first entered the SBC. The particles that entered the SBC through the West boundary were assumed to originate from the CC and through the East boundary were assumed to originate from the SCC. The particles that remained in the SBC during the 60-day reverse tracking time were identified as originating from the SBC. Particles that entered the SBC through the South boundary could have come from either the CC or the SCC. These calculations provided the daily percentage of water in the SBC originating from each of the four source water zones.

2.2 *Satellite observations of surface chlorophyll*

To quantify the spatial and temporal patterns of chlorophyll concentrations in the SBC, satellite-derived five-day composites of surface chlorophyll-a concentrations (Chl) with 1 km^2 resolution from 1998-2007 were used. The Chl data set was derived from three ocean color sensors, SeaWiFS, MODIS-Aqua, MODIS-Terra, and MERIS, assembled by the Scripps Photobiology Group at U.C. San Diego (Kahru et al. 2012, 2015, http://spg-satdata.ucsd.edu) and has been used in many studies of the California Current System (e.g. Kahru et al. 2012; McClatchie et al. 2016; Jacox et al. 2016b). Chl was used as a proxy for phytoplankton biomass in this study. While known biases can arise in the relationships between Chl and phytoplankton carbon biomass due to variability in phytoplankton physiological status, it is generally thought that phytoplankton biomass is the first-order determinant of Chl variability in productive coastal regions like the SBC (Behrenfeld et al. 2005; Siegel et al. 2013).

2.3 *Estimating nutrient concentrations*

The concentrations of macronutrients (nitrate + nitrite, phosphate, and silicate) tend to be highly correlated in the California EBUS, and nitrogen is typically the limiting macronutrient of phytoplankton production in this region (Messié and Chavez 2015; Deutsch et al. 2021). Many previous studies have shown a stable relationship between temperature and inorganic nitrogen in the SBC and SC Bight (Hayward and Venrick 1998; McPhee-Shaw et al. 2007; Omand et al. 2012; Snyder et al. 2020). In the California EBUS, prior work has shown that temperature is an adequate predictor of nitrate in areas, like the SBC, that are located within the same latitude and 50 km of the shoreline (Palacios et al. 2013; Jacox et al. 2018). Thus, the maximum available nitrate + nitrite concentrations (N_{max}) in the SBC surface layer were calculated using an empirical temperature to nitrate + nitrite relationship derived from water samples collected in the SBC and the 3D temperature solutions from the ROMS. Water sample data came from the CalCOFI (calcofi.org) and the UCSB Plumes and Blooms program (Fig. 1, Catlett et al. 2021). To avoid artifacts in the relationship due to nutrient uptake by phytoplankton, only water samples collected from depths below the surface layer, deeper than 30 m, were used. The empirical temperature to nitrate + nitrite relationship or N_{max} model was derived using 10,311 water samples collected at 14 stations in the SBC from depths of 35 m to 517 m over 1980-2018 (Fig. 1). To calculate N_{max} from ROMS temperature, the following fourth-order polynomial using a least squares fit was derived from the water sample data (Fig. 2):

$$N_{max} = -0.0108T^4 + 0.5899T^3 - 11.3447T^2 + 87.2050T - 196.3239$$

where N_{max} is the maximum available nitrate + nitrite concentration (μmol L^{-1}) and T (°C) is temperature in the surface layer, the top 30 m of the water column. To create a 3D N_{max} data set for the SBC surface layer, N_{max} was calculated from ROMS temperature horizontally at each grid cell and vertically every meter from the surface to 30 m depth every 6-hr for the 10-year modeling period, 1998-2007. N_{max} in the eddy was determined using the eddy detection scheme to identify the horizontal eddy area and then averaging N_{max} horizontally and vertically over the eddy area.

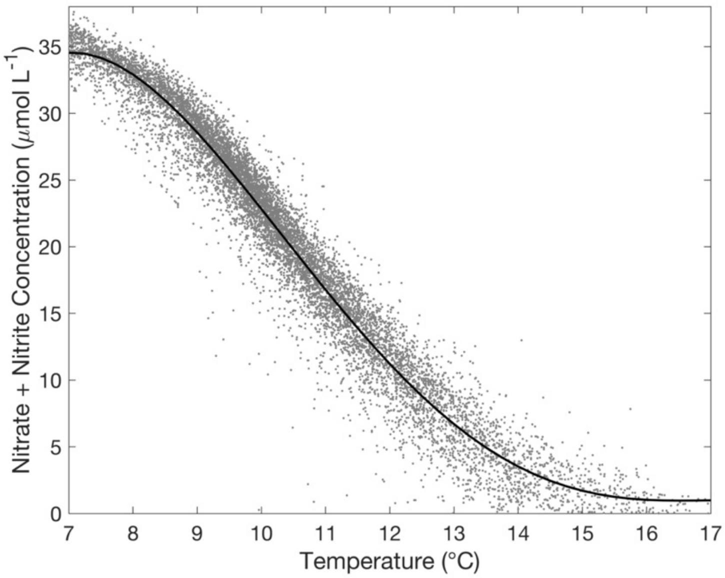

Figure 2: Nitrate + nitrite concentrations (μmol L^{-1}) vs. temperature (°C) from field samples of UCSB Plumes and Bloom and CalCOFI programs. Black line shows polynomial fit used to model N_{max}.

2.4 *Identifying N_{max} transport mechanisms*

Upwelling and eddy circulation are the primary processes associated with increased nutrients and Chl in the SBC (Anderson et al. 2006; McPhee-Shaw et al. 2007; Brzezinski and Washburn 2011). The strength of upwelling is usually quantified in EBUSs using surface wind stress or upwelling indices, which are a function of surface wind stress. However, the wind data used to force the ROMS was not available with the offline solutions of the SC Bight. Thus, to determine the presence and strength of the mechanisms transporting N_{max} into the SBC surface layer, Empirical Orthogonal Function (EOF) analysis was used on 2D depth-averaged N_{max} over the 10-year modeling period. The EOF method is a linear statistical method that identifies the spatiotemporal variability within a dataset by transforming the dataset into a set of empirical orthogonal functions or modes. The patterns of these modes can then be correlated with dynamic mechanisms in the ocean (Thomson and Emery 2014). The advantage of this method was that only mechanisms that were strong enough to transport elevated N_{max} into the surface layer were identified. This is particularly useful for the SBC where field studies have shown that while upwelling favorable winds tend to be most persistent in the spring, they occur intermittently all year round in the SBC (Dorman and Winant 2000; Oey et al. 2001). The first EOF mode explained 83.1% of the N_{max} variability. Representing a pattern of wind-driven upwelling, the mode 1 map (Fig. 3(a)) displayed a strong north-south gradient with the highest positive values along the mainland coast and lowest values along the north coast of the islands. Along the mainland coast, a west-east gradient is shown with higher positive values that extend farther from shore in the western than the eastern SBC, indicating that upwelling may be stronger in the western SBC. The second and third modes are associated with eddy circulation. The second EOF mode explained 6.0% of the N_{max} variability. Representing advection of elevated N_{max} water into the south-western SBC by eddy circulation, the mode 2 map (Fig. 3(b)) displayed the highest positive values in the south-western SBC with negative values along the mainland coast and eastern SBC. The third EOF mode explained 3.0% of the N_{max} variability. Representing retention of elevated N_{max} by eddy circulation in the western SBC, positive values in the mode 3 map (Fig. 3(c)) show a circular shape in the western SBC with negative values in the eastern SBC. By analyzing horizontal distributions of phytoplankton primary production (PPP) during seasonal channel-wide cruises from 2001-2006, Brzezinski and Washburn (2011) found that wind-driven upwelling was the primary process driving high PPP in the SBC and eddy circulation was the secondary process, supporting our results.

2.5 *Analysis*

Regulation of Chl in the SBC by upwelling and eddy circulation was assessed by comparing satellite observations of Chl to modeled parameters of N_{max}, RT, RT_{eddy}, source water zone, eddy size and lifespan, and N_{max} EOF modes. Physical controls on the spatiotemporal distribution of Chl in the SBC were investigated across the decadal, annual, interannual, and synoptic timescales. Where time-series of channel-wide mean values are presented, Chl and modeled parameters were horizontally averaged over the SBC and, when applicable, depth-averaged over the surface layer, the top 30 m of the water column. Horizontal distributions of modeled parameters were computed by depth-averaging over the surface layer. Where direct comparisons of Chl and modeled parameters are presented, Chl was interpolated to match the horizontal resolution of modeled parameters or modeled parameters were averaged over the 5-day Chl composites.

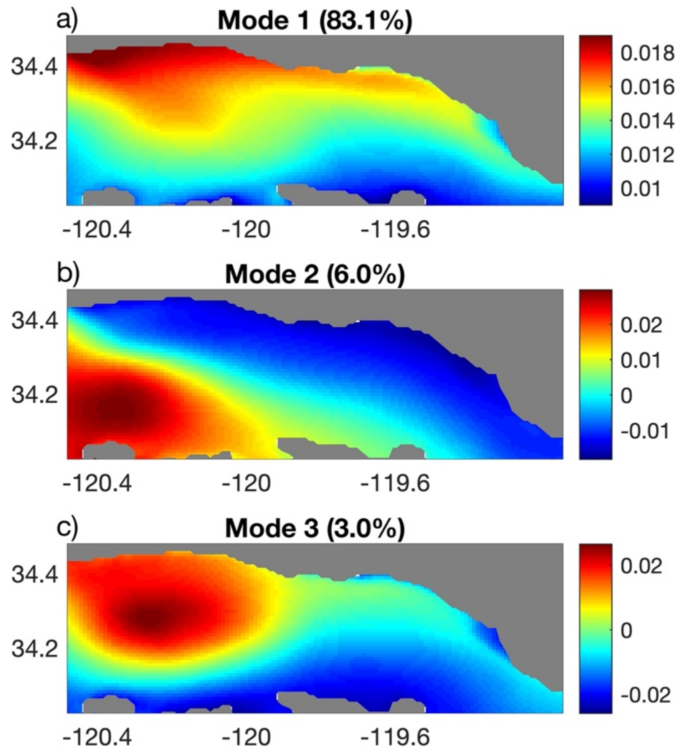

Figure 3: N_{max} Empirical Orthogonal Function maps for (a) mode 1, (b) mode 2, and (c) mode 3

3.0 Results

3.1 *Mean decadal horizontal distributions*

Fig. 4 shows the 10-year mean horizontal distributions of currents, Chl, N_{max}, and RT in the SBC. The mean current pattern in the surface layer (Fig. 4(a)) show that strong eddy circulation, centered mid-channel, dominates the mean circulation in the western SBC with weaker, primarily westward currents observed in the eastern SBC. The magnitude of the mean and maximum currents in Fig. 4(a) are 4 cm s^{-1} and 13 cm s^{-1} respectively. The highest mean Chl are observed in the western SBC where eddy circulation dominates and decreases to the north and east with the lowest values at the southeastern boundary (Fig. 4(b)). This spatial distribution of Chl has been observed in previous studies (Otero and Siegel 2004; Brzezinski and Washburn 2011; Henderikx Freitas et al. 2017). The mean Chl varies from 0.1-3.4 mg m^{-3} across 1 km^2 pixels. The spatial distribution of mean RT reflects the eddy circulation with the highest values of ~7 days in the central western SBC and lowest values of ~4 days in the southeastern SBC (Fig. 4(d)). The spatial distribution of mean N_{max} shows a distinct east-west gradient with the highest values of ~6 μmol L^{-1} observed in the western SBC and the lowest values of ~3 μmol L^{-1} observed in the eastern SBC. Unlike mean Chl and RT, the mean N_{max} distribution shows two distinct regions of high concentrations, a circular shaped region in the central western SBC and a region along the mainland coast in the north-western SBC. The circular region is located near the center of the eddy circulation (Fig. 4(a)) and coincides with the area of the highest mean Chl and RT (Fig. 4(b,d)).

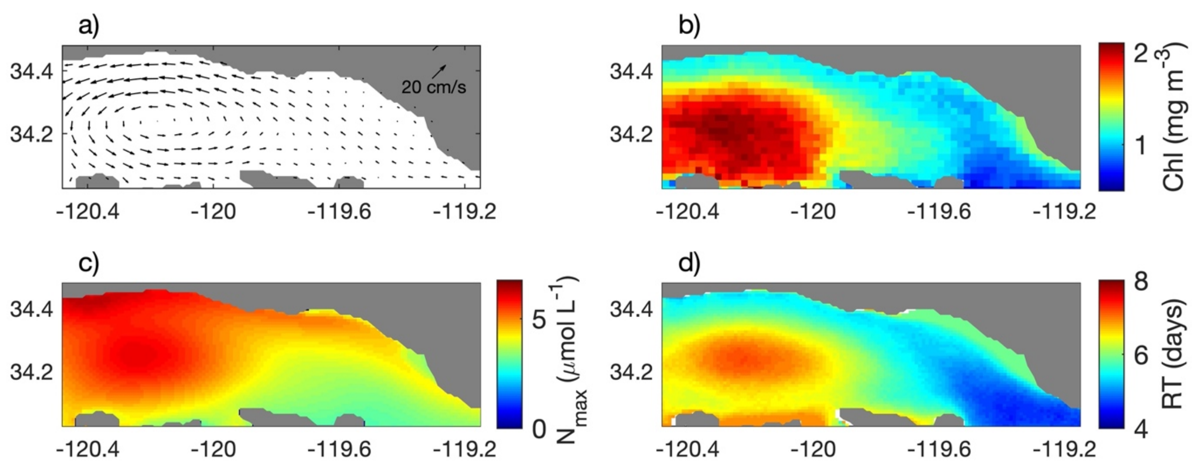

Figure 4: 10-year mean: (a) ROMS currents, (b) Chl (mg m^{-3}), (c) N_{max} (μmol L^{-1}), and (d) RT (days). N_{max}, RT, and currents are depth-averaged over the surface layer.

To show the relationship between mean N_{max}, RT, and Chl, mean Chl is shown as a function of mean N_{max} and RT in Fig. 5. Elevated mean Chl, defined by Chl greater than 1.4 mg m^{-3}, is found where mean N_{max} and RT are simultaneously greater than ~4 μmol L^{-1} and ~5.5 days, respectively. These conditions coincide with eddy circulation in the western SBC. In contrast, although mean N_{max} is elevated along the north-western mainland coast (Fig. 4(c)), the mean RT in this area is relatively short, less than 5.5 days, suggesting that N_{max} is advected away from the coast and into the open channel before elevated Chl can be produced. Thus, it appears that for long-term horizontal means, the elevated Chl in the SBC is being produced by a combination of long RT and high N_{max}.

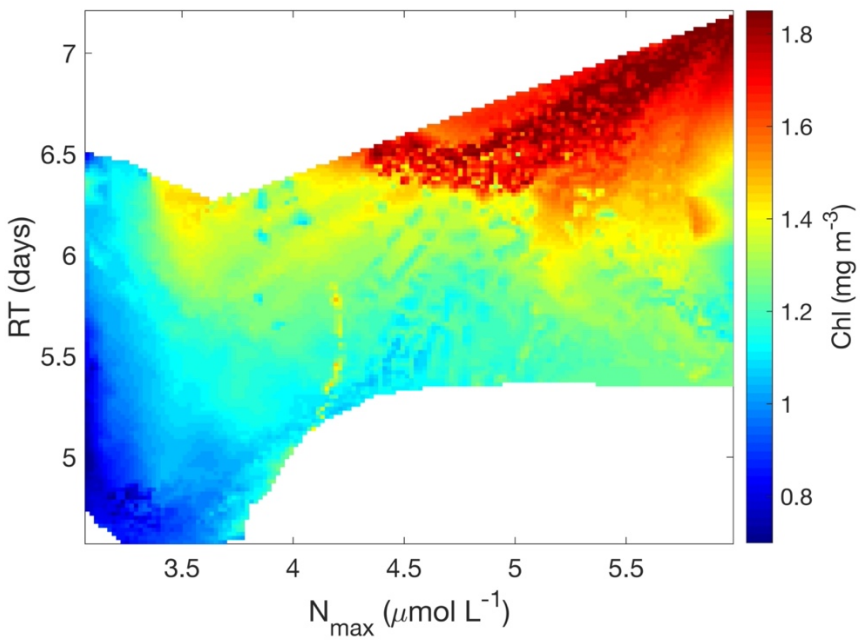

Figure 5: Chl (mg m^{-3}) as a function of N_{max} (μmol L^{-1}) and RT (days). White represents where Chl data are not available for N_{max}-RT combinations.

3.2 *Mean annual cycle*

Mean annual cycles of Chl, N_{max}, source water zone, eddy size, RT, and RT_{eddy} are displayed in Fig. 6. Chl shows a strong seasonal cycle with elevated values from March through June and maximum values of 3.8-5.4 mg m^{-3} in April and May (Fig. 6(a)). Low mean Chl is observed throughout the rest of the year, averaging 1.6 mg m^{-3}. This seasonal cycle of mean Chl in the SBC has been observed in prior studies (Shipe and Brzezinski 2001; Otero and Siegel 2004; Brzezinski and Washburn 2011; Henderikx Freitas et al. 2017). Mean N_{max} follows a seasonal cycle similar to mean Chl with elevated values in March through June and maximum values in April and May of 6.1-9.5 μmol L^{-1} (Fig. 6(b)). Low mean N_{max} is observed throughout the rest of the year with an average of 3.3 μmol L^{-1}. By averaging mean N_{max} in Fig. 6(b) over the 5-day composite window used for Chl (Fig. 6(a)), the annual cycle of mean Chl and N_{max} is shown to be highly correlated with a Pearson's squared correlation coefficient (r^2) of 0.83. Brzezinski and Washburn (2011) observed a similar relationship in the seasonal cycles of chlorophyll and nitrate in the SBC.

The mean annual cycles of physical properties, including source water zone, eddy size, RT, and RT_{eddy}, are shown in Fig. 6(c-f). Of these four physical properties, the annual cycle of source water from the West zone, representing the CC, is the most similar to the annual cycles of N_{max} and Chl (r^2 of 0.70-0.71) with maximum values of 40-65% from March to June (Fig. 6(c)). When the mean percent of water from the West zone is low in July-February, water in the SBC originates primarily from the East zone or the SCC, accounting for 45-61% of the SBC source water. The mean percent of water from inside the SBC ranges from 1-4% and from the South zone ranges from 5-8% throughout the year without a defined seasonal cycle.

Eddy circulation is detected throughout the year as indicated by the eddy size in Fig. 6(d)). Eddy size is directly proportional to the strength of eddy circulation and ranges from a few km^2 up to 450 km^2. The mean annual cycle of eddy size is much less pronounced than the mean annual cycles of Chl, N_{max}, and West zone source water and displays its largest values in May through October. These results are supported by field studies that observed the presence of eddy circulation most consistently in summer and fall (Harms and Winant 1998; Dever et al. 1998; Winant et al. 2003). Mean RT lacks a defined seasonal cycle and ranges from 4.2 to 7.5 days (Fig. 6(e)). The daily standard deviation of RT is fairly large, ranging from 2.0 to 3.2 days and indicating that for any single day the RT can vary widely. Mean RT_{eddy} (Fig. 6(f)) is consistently higher than the mean RT, ranging from 5.2 to 10.9 days over the year with a small standard deviation from 0.7-1.6 days and no clear seasonal cycle.

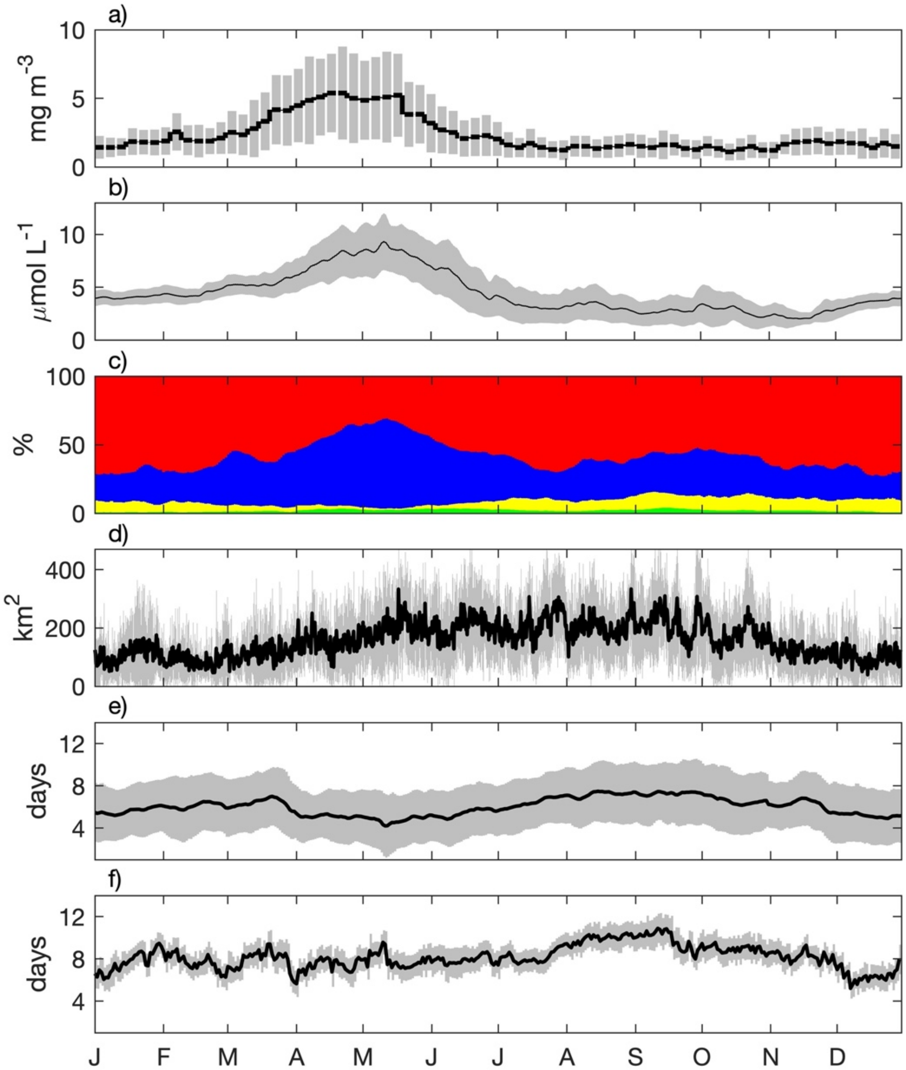

Figure 6: Mean annual cycle of (a) Chl (mg m^{-3}), (b) N_{max} (μmol L^{-1}), (c) source water zone (%) with West zone (blue), East zone (red), South zone (yellow), and SBC (green), (d) eddy size (km^2), (e) RT (days), and (f) RT_{eddy} (days). Gray areas show $\pm$ one standard deviation.

The mean annual cycle of the principal components for N_{max} EOF modes 1, 2 and 3 (PC1, PC2, and PC3) is shown in Fig. 7. From the EOF analysis in Section 2.4, the N_{max} transport mechanisms represented by each mode are (1) wind-driven upwelling, (2) advection of high N_{max} water into the south-western SBC by eddy circulation, and (3) retention of N_{max} within the SBC by eddy circulation. Mean PC1 shows a similar annual cycle as mean Chl, N_{max}, and West zone source water (Fig. 6(a-c)) with positive values in March through June and maximum values in April and May, reinforcing that upwelling is the primary transport process of N_{max} to the surface layer in spring. Although much smaller in variance than PC1, mean PC2 and PC3, representing the transport of N_{max} by eddy circulation, have peak positive values in late May and June, when PC1 decreases and then becomes negative (Fig. 7). This pattern suggests that as upwelling weakens, eddy circulation plays a larger role in transporting N_{max} in the SBC surface layer. Mean PC3 is consistently positive in June through October (Fig. 7(c)), which is when mean Chl and N_{max} are at their lowest and mean PC1 is negative.

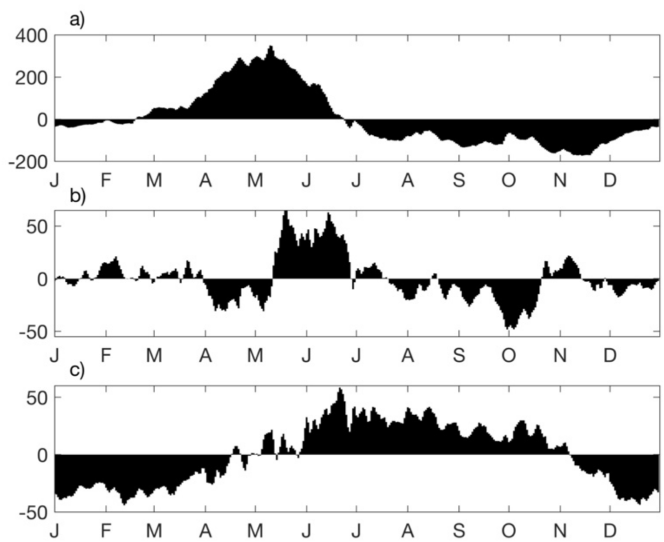

Figure 7: Mean annual cycle of principal components for N_{max} EOF: (a) mode 1, (b) mode 2, and (c) mode 3

To evaluate the spatial variability in the seasonal cycle of mean Chl, N_{max}, and RT, these parameters are averaged over the four seasons and shown in Fig. 8. The horizontal distributions of Chl and N_{max} in spring show the highest concentrations and are most similar to their decadal horizontal means (Fig. 4(b,c)), implying that spring activity is driving the decadal mean distributions. Both Chl and N_{max} in spring (Fig. 8(b,f)) display distinct along channel gradients with high concentrations in the western SBC, low concentrations in the eastern SBC, and maximum concentrations in the central western SBC where decadal mean eddy circulation is observed (Fig. 4(a)). Compared to spring, Chl and N_{max} display decreasing concentrations throughout the SBC in summer and fall, although both parameters continue to show along-channel gradients with the highest concentrations in the western SBC. In contrast, RT displays high values in the western SBC of similar magnitude throughout the year with the spatial distribution of RT varying in shape with the season (Fig. 8(i-l)). Although eddy circulation is present throughout the year, the eddy is not stationary and moves primarily along-channel in the western SBC with a tendency to propagate westward (Harms and Winant 1998; Beckenbach and Washburn 2004; Simons et al. 2015). Shown in Fig. 8(i-l), the oval shape of the longest RT, greater than approximately 6 days, reflects the along-channel movement of the eddy, which is smallest in spring, largest in summer and fall, and at its least constrained in winter. Overall, Fig. 8 emphasizes the need for both high N_{max} and long RT to be present to produce elevated Chl.

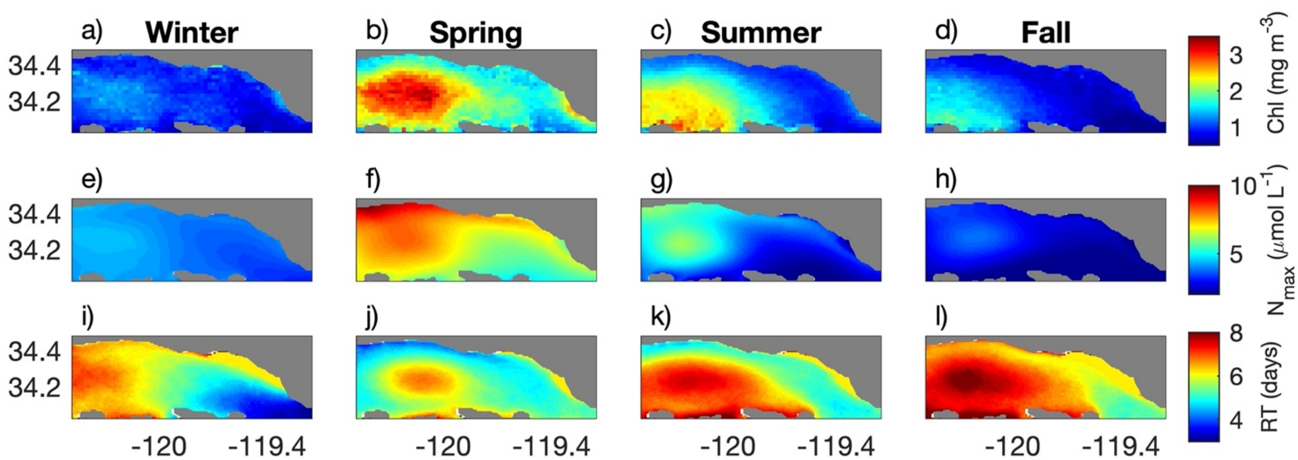

Figure 8: Mean seasonal cycle of Chl (mg m^{-3}) for (a) winter (Dec-Feb), (b) spring (Mar-May), (c) summer (Jun-Aug), and (d) fall (Sep-Nov), N_{max} (μmol L^{-1}) for (e) winter, (f) spring, (g) summer, and (h) fall, and RT (days) for (i) winter, (j) spring, (k) summer, and (l) fall

3.3 *Interannual variations in the spring upwelling period*

Time-series of Chl and N_{max} over the 10-year modeling period are shown in Fig. 9(a,b). Although varying in magnitude between years, the maximum Chl and N_{max} are consistently observed in the spring. Similarly, PC1 or upwelling strength shows the largest positive values in the spring (Fig. 10(a)). Based on these results as well as the mean annual cycles, our interannual analysis focuses on the spring upwelling period (SUP), the time of year with the strongest upwelling and highest Chl and N_{max}. The SUP is defined by contiguous positive values of PC1 that occur in February through July. From 1998 to 2007, the SUP ranges in length from 42 to 127 days with an annual average of 76 days (Table 1, Fig. 10(a)). Mean values of Chl, N_{max}, PC1, RT and RT_{eddy} for yearly SUPs are shown in Table 1. For every year except 1998 and 1999 when a strong ENSO cycle occurred, the SUP is associated with elevated mean Chl ranging from 3.7 to 8.3 mg m^{-3} and elevated mean N_{max} ranging from 6.0 to 10.7 μmol L^{-1} (Table 1, Fig. 9(a,b)). Mean Chl and N_{max} from times of the year other than the SUP are 1.6 mg m^{-3} and 3.3 μmol L^{-1} respectively.

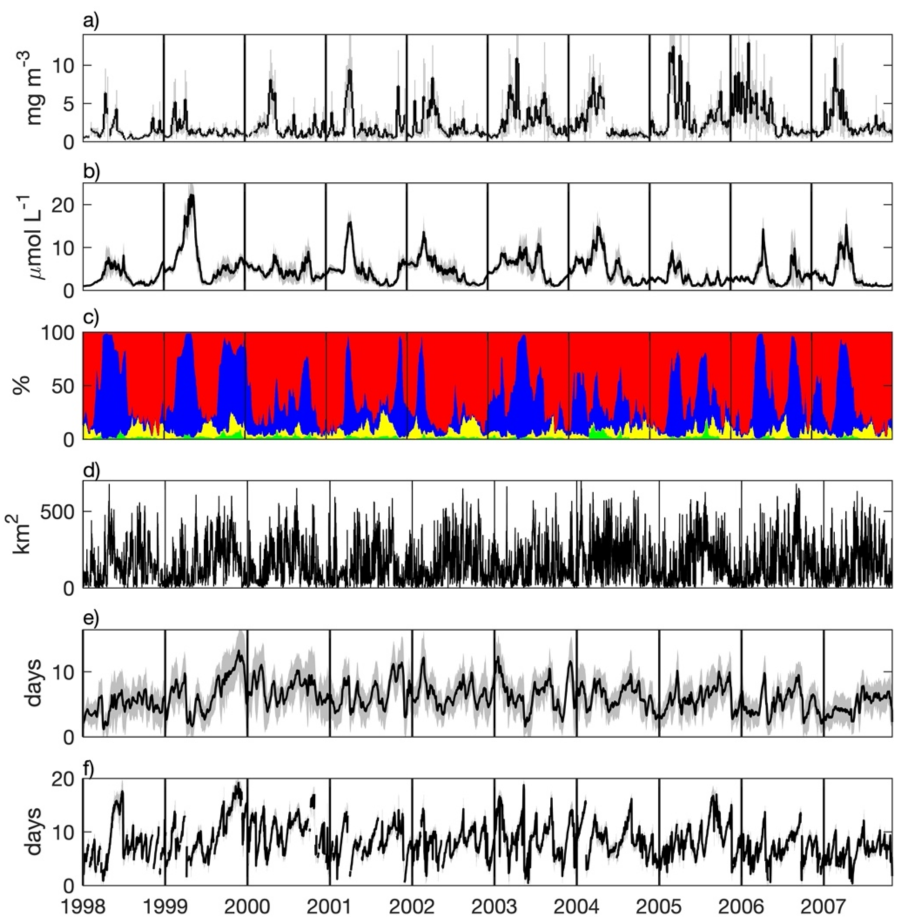

Figure 9: SBC time-series of (a) Chl (mg m^{-3}), (b) N_{max} (μmol L^{-1}), (c) source water zone (%) with West zone (blue), East zone (red), South zone (yellow), and SBC (green), (d) eddy size (km^2), (e) RT (days), and (f) RT_{eddy} (days). Gray areas show $\pm$ one standard deviation.

Parameter	Units	Year										Yearly Mean
		1998	1999	2000	2001	2002	2003	2004	2005	2006	2007	
Start date		Apr 19	Feb 9	Apr 24	Mar 23	Feb 19	May 13	Mar 21	Mar 27	May 3	Apr 18	Mar 28
End date		Jul 7	Jun 15	Jun 4	May 20	May 20	Jul 19	Jun 23	May 23	Jun 16	Jul 19	Jun 15
Length	days	92	127	42	59	91	68	95	58	45	83	76
Chl	mg m^{-3}	2.2	2.2	4.4	5.3	3.7	4.0	4.9	8.3	4.0	4.2	4.3
N_{max}	μmol L^{-1}	5.6	12.5	6.0	10.7	8.2	7.4	9.4	6.0	7.6	8.7	8.2
Upwelling strength (PC1)		88	561	103	432	263	218	363	119	218	291	266
RT	days	4.8	5.5	6.4	5.9	6.5	4.9	6.2	5.3	4.7	5.0	5.5
RT_{eddy}	days	11.1	8.1	10.3	6.6	7.0	7.1	8.4	8.5	6.0	6.5	8.0
MEI		1.57	-0.88	-0.10	0.04	0.32	0.07	0.31	0.67	0.57	-0.13	0.3
Maximum eddy lifespan	days	56	30	27	11	22	22	11	6	20	8	21
Eddy size upwelling	km^2	263	116	156	130	62	80	201	137	131	159	144
Eddy size relaxation	km^2	131	131	237	209	131	242	285	208	282	224	208
Maximum RT_{eddy}	days	17.6	13.8	12.9	9.2	14.0	13.5	13.2	11.5	8.4	12.1	12.6
N_{max} in eddy - N_{max}*	μmol L^{-1}	1.7	8.5	6.4	7.3	5.0	4.4	6.9	4.1	8.4	5.4	5.8
Maximum N_{max} Flux	μmol L^{-1} day^{-1}	3.8	13.8	1.7	4.1	2.1	4.4	3.7	2.5	3.7	4.7	4.4

Table 1: Yearly data for the spring upwelling period (SUP). Mean values are displayed unless otherwise indicated. *At the end of the SUP.

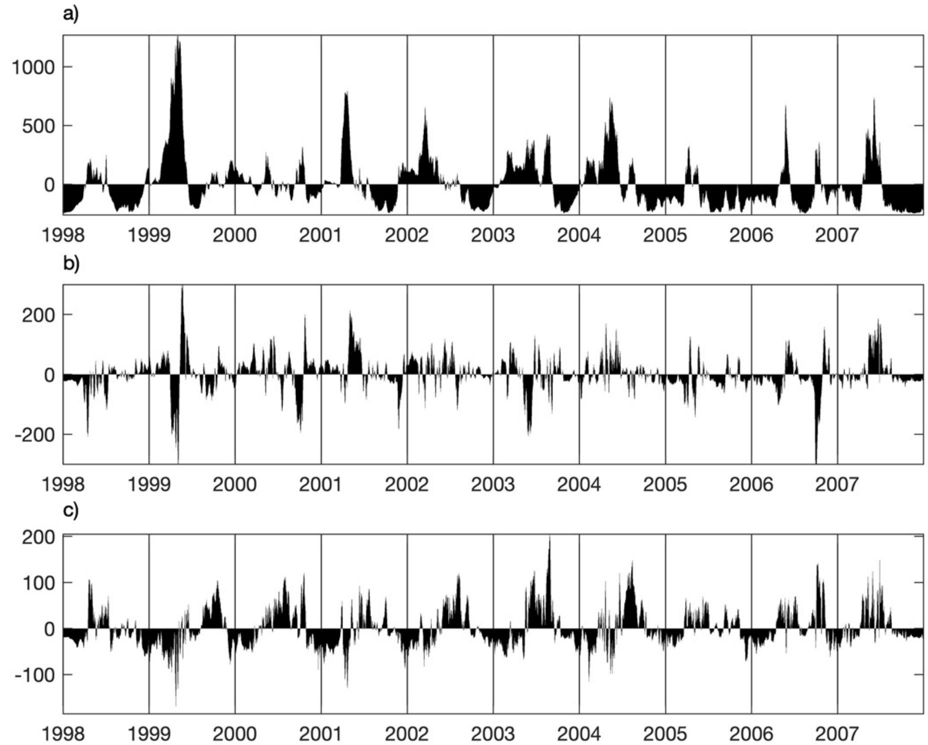

Figure 10: Principal components for N_{max} EOF: (a) mode 1, (b) mode 2, and (c) mode 3.

Section 3.3.1 ***Typical spring upwelling period***

The strength and timing of N_{max} transport processes during the SUP are critical to understanding how upwelling and eddy circulation regulate Chl in the SBC. The SUP consists of three main phases; (1) the upwelling phase, when upwelling starts and then increases in strength, (2) the transition phase, when upwelling transitions from increasing to decreasing strength, and (3) the relaxation phase, when upwelling strength declines until the end of the SUP. To examine these three phases, time-series of Chl, N_{max}, PC1, eddy size, RT, and RT_{eddy} during a typical SUP are examined (Figs. 11(a-f) and 12). The 2001 SUP is presented as a typical SUP for several reasons. First, PC1 displays a clear three phase cycle. Second, the 2001 SUP has the best agreement between modeled and observed temperature in the SBC (see SI). Third, the 2001 SUP has a neutral multivariate ENSO index (MEI), which tracks El Niño and La Niña events in the Pacific Ocean (Table 1, Fig. S1). Although the following analysis focuses on the 2001 SUP, the 2000 and 2002-2007 SUPs display similar results, which are shown for comparison in Table 1 and Figs. 9 and 10.

In the upwelling phase of the 2001 SUP, upwelling begins and increases in strength as displayed by the increasing values of PC1 from March 23 to April 12 in Fig. 11(c). Chl and N_{max} also steadily increase during this phase (Fig. 11(a,b)). The horizontal advection of upwelled water from the CC into the SBC results in a rapid drop in RT (Fig. 11(e)) and little to no eddy circulation as represented by the small eddy size (Fig. 11(d)). Shown for April 2nd in Fig. 12(a,d), the spatial relationship of N_{max} and RT during the upwelling phase displays the intrusion of high N_{max} water from the west, which corresponds to a shortened RT and the absence of eddy circulation. Next in the transition phase, upwelling strength stops increasing as shown by the plateauing values of PC1 from April 13 to 22 in Fig. 11(c). This coincides with maximum Chl and N_{max} and increasing RT and eddy size (Fig. 11 (a-b,d-e)). During the transition phase on April 14th, the horizontal distribution of N_{max} shows values greater than 10 μmol L^{-1} across the entire SBC with the highest concentrations along the mainland coast (Fig. 12(b)). The horizontal distribution of RT on April 14th shows increased RT and eddy circulation compared to the upwelling phase as advection from the west weakens (Fig. 12(e)).

The relaxation phase, the last phase of the SUP, displays the greatest deviation from typical upwelling-relaxation cycles in EBUSs due to the presence of eddy circulation. In this phase, upwelling strength decreases, shown by the steady decline in PC1 from April 23 to May 20 (Fig. 11(c)). Chl and N_{max} similarly decline during this phase (Fig. 11(a,b)). Horizontal distributions of N_{max} and RT on May 12th (Fig. 12(c,f)) show that the influx of high N_{max} water from the west has stopped and eddy circulation has strengthened. Eddy circulation has trapped high N_{max} water in the western SBC as shown by the high N_{max} and long RT located within the eddy area (Fig. 12(c,f)). N_{max} within the eddy, shown in Fig. 11(b), is similar in magnitude to N_{max} in the SBC during the upwelling and transition phases, but is greater than N_{max} in the SBC by 3-7 μmol L^{-1} throughout the relaxation phase as eddy circulation retains high N_{max} water. The largest difference between N_{max} within the eddy and N_{max} in the SBC of 7.3 μmol L^{-1} is observed at the end of the SUP. Similar to the 2001 SUP, the other typical years, 2000 and 2002-2007, all show an increase in eddy size from the upwelling to the relaxation phase and N_{max} in the eddy higher than N_{max} in the SBC at the end of SUP (Table 1).

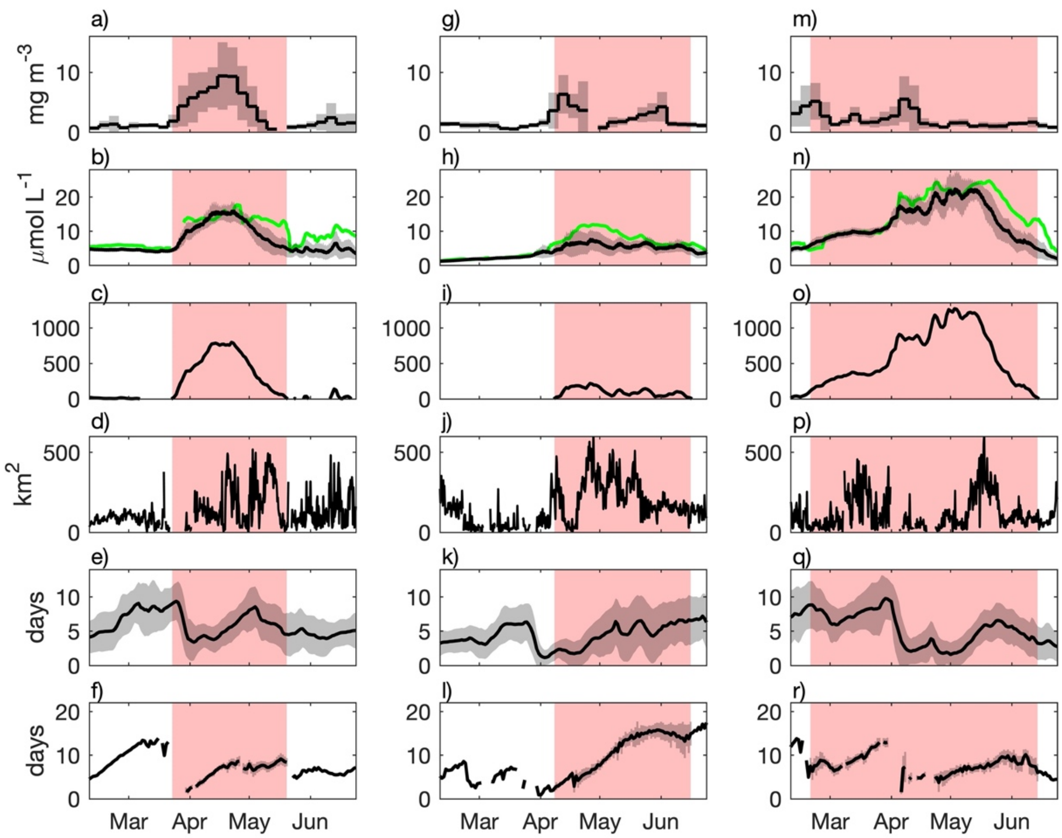

Figure 11: Chl (mg m^{-3}) for (a) 2001, (g) 1998, and (m) 1999; N_{max} (μmol L^{-1}, black line) and N_{max} in eddy (μmol L^{-1}, green line) for (b) 2001, (h) 1998, and (n) 1999; Positive values of PC1 for (c) 2001, (i) 1998, and (o) 1999; eddy size (km^2) for (d) 2001, (j) 1998, and (p) 1999; RT (days) for (e) 2001, (k) 1998, and (q) 1999; RT_{eddy} (days) for (f) 2001, (l) 1998, and (r) 1999. Pink areas identify the SUP. Gray areas show ± one standard deviation.

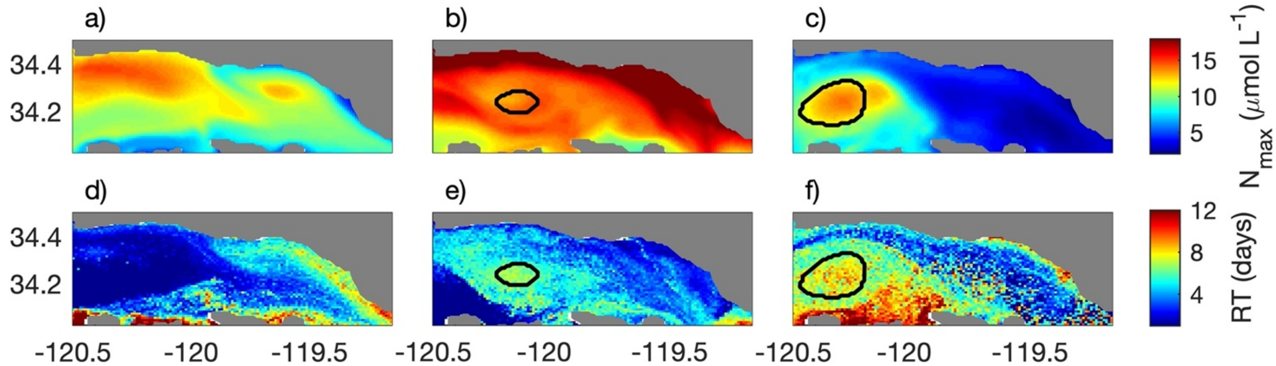

Figure 12: N_{max} (μmol L^{-1}) for (a) upwelling phase on April 2, 2001, (b) transition phase on April 14, 2001, and (c) relaxation phase on May 12, 2001. RT (days) for (d) upwelling phase on April 2, 2001, (e) transition phase on April 14, 2001, and (f) relaxation phase on May 12, 2001. Black line identifies the eddy area. N_{max} and RT have been depth-averaged over the surface layer.

3.3.2 *Spring upwelling period during extreme El Niño and La Niña conditions*

Patterns of upwelling and eddy circulation during 1998 and 1999 SUPs deviate the most from the typical years and coincide with an exceptionally strong ENSO cycle, an extreme El Niño event in 1998 followed by an extreme La Niña event in 1999. The SUP in both 1998 and 1999 have anomalously low mean Chl of 2.2 mg m^{-3}, which is 40-74% lower than the other years of 2000-2007 in the study period (Table 1 and Fig. 11(g,m)). While strong El Niño events historically disrupt primary productivity in the California EBUS, La Niña events are often associated with enhanced upwelling and phytoplankton accumulation (Bograd et al. 2000; Schwing et al. 2000; Bograd and Lynn 2001).

The 1998 SUP coincided with an extreme El Niño, which resulted in a mean PC1, upwelling strength, and N_{max} of 88 and 5.6 μmol L^{-1} respectively, the lowest of all yearly SUPs (Table 1, Fig. 11(h,i)). Taking place from April 19 to July 7, the 1998 SUP does not display distinct phases of upwelling, transition, and relaxation, but instead shows very weak upwelling of similar magnitude throughout the SUP. In addition, the 1998 SUP exhibits an anomalous pattern of eddy circulation compared to the typical SUPs of 2000-2007. Unlike a typical SUP where eddy circulation increases in strength from the upwelling phase to the relaxation phase, eddy circulation is strong and continuous for most the 1998 SUP as shown by the eddy size in Fig. 11(j). During the 1998 SUP, eddy circulation displays a lifespan, defined as a continuously tracked eddy, of 56 days from May 3 to June 28. Present for 60% of the 1998 SUP, this eddy lifespan is twice as long as the longest eddy lifespan for the other SUPs (Table 1) and almost five times longer than the mean SUP eddy lifespan of 12 days. RT_{eddy} is exceptionally long with an average of 14.3 days over the 56-day eddy lifespan, which is 79% greater than the SUP mean eddy lifespan of 8 days (Table 1). Horizontal distributions of N_{max} and RT on May 7th, the midpoint of the 1998 SUP, show that N_{max} within the eddy is only slightly greater than N_{max} outside of the eddy and that RT is much higher within the eddy than outside (Fig. 13(a,c)). These horizontal distributions are distinctly different from all phases of the 2001 SUP (Fig. 12). These results imply that in the presence of very weak upwelling, prolonged periods of eddy circulation produce long RT, but not high N_{max} or elevated Chl.

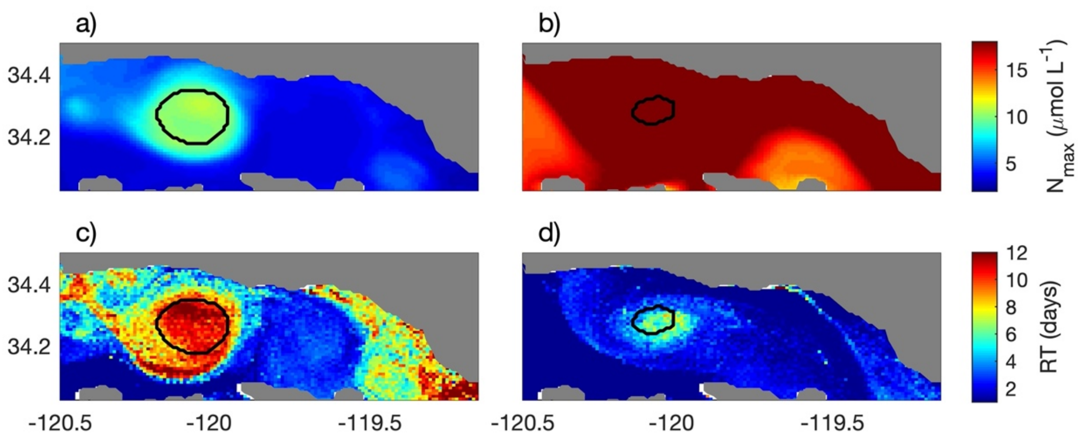

Figure 13: N_{max} (μmol L^{-1}) on (a) May 7, 1998 and (b) May 1, 1999. RT (days) on (c) May 7, 1998 and (d) May 1, 1999. Black line identifies the eddy area. N_{max} and RT have been depth-averaged over the surface layer.

In contrast, 1999 is an extreme La Niña year with record high upwelling for the entire California EBUS (Schwing et al. 2000). This strong upwelling is reflected in the model predictions for the 1999 SUP, which has the highest mean PC1, upwelling strength, of 561 and N_{max} of 12.5 μmol L^{-1} of all the SUPs (Table 1). The 1999 SUP is the longest SUP, lasting 127 days from February 9 to June 15. Although the 1999 SUP has unusually high N_{max}, it does not show elevated Chl with a mean Chl of 2.2 mg m^{-3}, the same as the 1998 SUP, which has the weakest upwelling (Table 1). Similar to the 2001 SUP, the 1999 SUP shows three distinct phases of upwelling, transition, and relaxation shown by the patterns of N_{max} and PC1 (Fig. 11(n,o)). However, eddy circulation deviates from the typical SUPs by remaining small throughout the transition phase, which is 38 days from April 7 to May 15 (Fig. 11(p)). During the 1999 transition phase, upwelling strength (PC1) and N_{max} are atypically high, averaging 1,044 and 18.9 μmol L^{-1} respectively (Fig. 11(n,o)), but RT is unusually low, averaging only 2.6 days (Fig. 11(p). This very low RT indicates that water is being advected through the SBC very quickly. To approximate the N_{max} flux through the SBC, N_{max} is divided by RT for all of the SUPs. All SUPs have a daily N_{max} flux of 4.7 μmol L^{-1} day^{-1} or less except for the 1999 SUP transition phase where N_{max} flux ranges from 4.8 to 13.8 μmol L^{-1} day^{-1} (Table 1). The horizontal distributions of N_{max} and RT during the transition phase on May 1, 1999 (Fig. 13(b,d)) are very different than those of the 2001 SUP transition phase (Fig. 12(b,e)) with unusually high N_{max} and low RT throughout the SBC. The eddy is also small on May 1st, containing only slightly elevated RT (Fig. 13 (b,d)). These results suggest that the exceptionally strong upwelling in 1999 advected nutrients through the SBC too quickly for Chl accumulation.

4.0 Discussion and Conclusions

Our results suggest that spring Chl in the SBC is regulated by the coupling of upwelling and eddy circulation and that elevated spring Chl requires the presence of both high N_{max} from upwelling and long RTs from eddy circulation at mean decadal (Figs. 4-5), mean annual (Figs. 6-8), interannual (Figs. 9-11), and synoptic timescales (Figs. 12-13). Unlike most of the coast in the SC Bight that is dominated by the warm poleward flowing SCC, the SBC is a transition zone where the cold equatorward flowing CC and the warm poleward flowing SCC meet, which, along with the bathymetry, creates a pattern of cyclonic eddy circulation (Hickey 1993; Harms and Winant 1998; Oey et al. 2004). Our results show that eddy circulation is present throughout the year in the SBC (Figs. 6(d) and 9(d)) and a critical process driving the Chl hotspot in SBC.

4.1 *Upwelling and eddy circulation stimulate a productivity hotspot in the SBC*

In the California EBUS, the time required after an upwelling event for phytoplankton to deplete the surface ocean of new nutrients is 3-10 days (Dugdale et al. 1997; Botsford et al. 2006; Wilkerson et al. 2006; Krause et al. 2013). Our study predicts a 10-year mean RT of 6.0 $\pm$ 2.7 days (mean $\pm$ 1 standard deviation) in the SBC, which meets the above criteria for nutrient uptake. In addition, eddy circulation creates a horizontal oval pattern of long mean RTs in the western SBC, which persists in the spring, summer, and fall and correlates with similar patterns of high mean N_{max} and Chl in the spring (Fig. 8). When comparing the 10-year mean horizontal distributions of RT and N_{max} to Chl, both elevated RT and N_{max} are required to produce high Chl, greater than ~1.4 mg m^{-3}, with minimum threshold values of ~4.0 μmol L^{-1} for N_{max} and ~5.5 days for RT (Fig. 5).

On a mean annual scale, the modeling predicts the strongest upwelling in the spring (Fig. 7(a)), which coincides with elevated Chl, high N_{max}, and a large influx of water from the CC (Fig. 6(a-c)). These results reflect previous studies of the SBC that observed high Chl, phytoplankton primary production, and nutrients in the spring followed by low values the rest of the year (Otero and Siegel 2004; Brzezinski and Washburn 2011; Henderikx Freitas et al. 2017). The mean annual SUP ranges from March to June as determined by PC1 (Fig. 7(a)) and coincides with the transport of N_{max} by eddy circulation from late-May to June, represented by PC2 and PC3 (Fig. 7(b-c)). While mean RT and RT_{eddy} remain above the nutrient uptake and depletion timescales throughout the year (Fig. 6(e,f)), mean elevated Chl is only observed during the SUP when mean N_{max} is high. While positive PC2 and PC3 are present during the SUP (Fig. 7(b,c)), they are also positive at other times of the year when elevated Chl is not observed. This indicates that eddy circulation without upwelling is unlikely to transport new nutrients into the surface layer in sufficient quantities to stimulate elevated Chl on the spatial scale of this study.

On an interannual scale, the SUP is observed for every year of the 10-year modeling period, beginning as early as February and ending as late as July. The SUP ranges in length from 1-4 months and occurs most frequently in April and May. A typical SUP consists of three phases; upwelling, transition, and relaxation. When upwelling increases in strength during the upwelling phase, eddy circulation is weak and RT is short due to the strong westward advection of high N_{max} water from the CC. During the transition and relaxation phases when upwelling strength plateaus and then weakens, eddy circulation strengthens, and RT increases. Consequently, eddy circulation traps and retains nutrients introduced by upwelling in the SBC. This process is clearly demonstrated by N_{max} in the eddy remaining elevated throughout the relaxation phase while N_{max} outside of the eddy decreases (Figs. 11(b) and 12(c), Table 1). Overall, eddy retention of high N_{max} water during the relaxation phase appears to be a critical factor in regulating the Chl hotspot in the SBC.

Due to its sheltered coastline, upwelling in the SC Bight is weak and intermittent compared to the Northern and Central California EBUS (Winant and Dorman 1997; Dorman and Winant 2000; Strub and James 2000). However, the SBC contains Chl in the spring that is higher than the rest of the SC Bight and similar in magnitude the coast north of Point Conception (Fig. 1, Mantyla et al. 1995; Henderikx Freitas et al. 2017; Kilpatrick et al. 2018). We hypothesize that eddy circulation when coupled with the relatively weak upwelling amplifies the seasonal Chl cycle in the SBC.

4.2 *ENSO events point toward implications for understanding climate-driven changes in upwelling*

There has been much speculation about the impact of climate change on the intensity of upwelling in EBUSs and how this will affect phytoplankton primary production (Bograd et al.

2023). ENSO is one of the major drivers of interannual variability in the SC Bight and has been observed to disrupt typical patterns in spring primary productivity (Bograd and Lynn 2001; Shipe and Brzezinski 2001; Shipe et al. 2002). In 1998, an extreme El Niño event occurred in the California EBUS, producing unusually weak upwelling, unseasonably warm water temperatures, and record low Chl (Lynn et al. 1998; Kudela and Chavez 2002). For the 1998 SUP in the SBC, the mean Chl was less than 50% of the yearly average and only slightly greater than background levels (Table 1). The model predicts the weakest upwelling and the lowest N_{max} for the 1998 SUP of the 10-year modeling period. In addition to weak upwelling, the pattern of eddy circulation deviates significantly from a typical SUP with strong continuous eddy circulation lasting for two months. This is the longest period of uninterrupted eddy circulation for all SUPs and is very unusual as the average eddy lifespan for the SUPs is only 12 days. Although the prolonged eddy circulation produces record long RT_{eddy} during the 1998 SUP, neither the strong eddy circulation or the weak upwelling transports sufficient N_{max} into the surface layer to produce elevated Chl.

Following the extreme El Niño in 1998, an extreme La Niña event occurred in 1999 with record high upwelling throughout the California EBUS (Bograd et al. 2000; Schwing et al. 2000). The 1999 SUP displays the strongest upwelling of the 10-year modeling period with a mean PC1 and N_{max} that are 100% and 50% greater respectively than the yearly average (Table 1). However, the strong upwelling did not produce elevated Chl as the 1999 SUP has the lowest mean Chl of the 10-year modeling period, matching the mean Chl of the 1998 SUP (Table 1). During the 1999 SUP, maximum upwelling strength and N_{max} occurs in April and May. In contrast, eddy circulation and RT are unusually small during these months due to the fast eastward flow of CC water entering the SBC. Our results show that the flux of N_{max} through the SBC in April and May of 1999 is greater than the maximum flux of N_{max} for all other SUPs. Thus, we hypothesize that the unusually strong upwelling resulted in anomalously low Chl by suppressing eddy circulation and RT to the point where phytoplankton biomass was not able to accumulate in the SBC.

Conceptual models of shelf chlorophyll for the Northern and Central California EBUS suggest that maximum shelf chlorophyll occurs when the strength of upwelling favorable winds fall into an optimal mid-range between weak and strong (Botsford et al. 2003; Stone et al. 2020). This optimal upwelling injects sufficient nutrients into the surface layer to stimulate phytoplankton growth, while allowing adequate retention of upwelled waters for phytoplankton nutrient uptake and accumulation. Work by Jacox et al. (2016a) also supports this conceptual model with ROMS simulations of the Northern and Central California EBUS for 13 years including the 1998 El Niño and 1999 La Niña. By comparing the SUPs from the typical years to the two anomalous years of 1998 and 1999, we propose the following conceptual model for the SBC SUP on how Chl is regulated by the interaction of upwelling and eddy circulation. High Chl production in typical years is associated with optimal conditions of intermediate upwelling strength and N_{max} flux, which allows sufficient injection of N_{max} into the surface layer and eddy circulation to retain N_{max} in the SBC. However, when upwelling strength and N_{max} flux are greater than optimal conditions, eddy circulation is too weak to retain N_{max} in the SBC, and N_{max} is advected out of the SBC too quickly to produce high Chl. In contrast, when upwelling strength and N_{max} flux are below optimal conditions, N_{max} is too low to produce high Chl, and strong eddy circulation does not contribute enough N_{max} to the surface layer to produce high Chl.

Decadal climate oscillations may also impact our observations, but our ability to resolve these impacts is limited by the relatively short modeling period. In particular, the North Pacific Gyre Oscillation (NPGO) is thought to drive decadal variations in the southern CC ecosystem, including the SBC, but remained in a cold phase for most of the study period except for a short warm phase in 2005 and 2006 (Di Lorenzo et al. 2008; Catlett et al. 2021). The 2005 and 2006 SUPs are associated with N_{max} slightly below, but close to, average (Table 1), suggesting that the NPGO warm phase did not exert a significant influence on SBC upwelling strength. Although

Chl is above average for the 2005 SUP and below average for the 2006 SUP, highly anomalous Chl are not observed in either year. Previous observations showed that anomalous advection of SCC water into the SBC in 2005 and 2006 was associated with unusual dinoflagellate bloom events (Catlett et al. 2021). However, since the multi-decadal climate variability and the variability in phytoplankton composition on Chl cannot be resolved in the present study, future work should be conducted on the influence of decadal climate oscillations on the SBC.

Climate-driven changes in upwelling patterns in EBUSs are a major ecological concern (Bograd et al. 2023). The weak upwelling and warm temperatures of the 1998 El Niño represent conditions of long marine heatwaves, extended periods of unusually warm water temperatures, which have detrimental effects on the ecology and have become more frequent in the SBC and EBUSs globally due to climate change (Cavole et al. 2016; Benthuysen et al. 2020; Michaud et al. 2022). In contrast, Bakun (1990) hypothesized that under climate change, upwelling rates in EBUSs would intensify due to the differential heating response between land and water. More recent studies have shown that upwelling has intensified across some EBUSs, although observed changes are spatially variable (Sydeman et al. 2014; Wang et al. 2015). For the California EBUS, a trend in increased upwelling strength has been observed for the Northern and Central California EBUS, but is not for the Southern California EBUS including the SC Bight (Jacox et al. 2015; Quilfen et al. 2021). The La Niña conditions in 1999 represent the potential consequences for the SBC and other coastal zones when strong upwelling reduces RT to an extent that does not allow nutrient uptake by phytoplankton. As the balance between the upwelling and eddy circulation regulates the Chl hotspot in the SBC, disruptions to this balance, such as those shown during the 1998 and 1999 SUPs, provide a framework for predicting the ecological consequences of climate-driven changes in upwelling for the future.

Acknowledgements

This research was supported by the National Science Foundation Biological Oceanography Program (OCE-2023693).

References

Anderson C, Brzezinski M, Washburn L, Kudela R (2006) Circulation and environmental conditions during a toxigenic Pseudo-nitzschia australis bloom in the Santa Barbara Channel, California. Mar Ecol Prog Ser 327:119–133. https://doi.org/10.3354/meps327119

Bakun A (1990) Global climate change and intensification of coastal ocean upwelling. Science 247:198–201. https://doi.org/10.1126/science.247.4939.198

Beckenbach E, Washburn L (2004) Low-frequency waves in the Santa Barbara Channel observed by high-frequency radar. J Geophys Res 109:C02010. https://doi.org/10.1029/2003JC001999

Beers JR, Trent JD, Reid FMH, Shanks AL (1986) Macroaggregates and their phytoplanktonic components in the Southern California Bight. J Plankton Res 8:475–487. https://doi.org/10.1093/plankt/8.3.475

Behrenfeld MJ, Boss E, Siegel DA, Shea DM (2005) Carbon-based ocean productivity and phytoplankton physiology from space. Global Biogeochem Cycles 19:GB1006. https://doi.org/10.1029/2004GB002299

Benthuysen JA, Oliver ECJ, Chen K, Wernberg T (2020) Editorial: Advances in understanding marine heatwaves and their impacts. Front Mar Sci 7:147. https://doi.org/10.3389/fmars.2020.00147

Bograd S, Digiacomo PM, Durazo R, et al (2000) The State of the California Current, 1999-2000: Forward to a new regime? Calif Coop Fish Invest Rep 41:26–52

Bograd SJ, Jacox MG, Hazen EL, et al (2023) Climate change impacts on Eastern Boundary Upwelling Systems. Annu Rev Mar Sci 15:303–328. https://doi.org/10.1146/annurev-marine-032122-021945

Bograd SJ, Lynn RJ (2001) Physical-biological coupling in the California Current during the 1997-99 El Niño-La Niña Cycle. Geophys Res Lett 28:275–278. https://doi.org/10.1029/2000GL012047

Botsford LW, Lawrence CA, Dever EP, et al (2006) Effects of variable winds on biological productivity on continental shelves in coastal upwelling systems. Deep Sea Res Part II: Top Stud Oceanogr 53:3116–3140. https://doi.org/10.1016/j.dsr2.2006.07.011

Botsford LW, Lawrence CA, Dever EP, et al (2003) Wind strength and biological productivity in upwelling systems: an idealized study. Fish Oceanogr 12:245–259. https://doi.org/10.1046/j.1365-2419.2003.00265.x

Bray NA, Keyes A, Morawitz WML (1999) The California Current system in the Southern California Bight and the Santa Barbara Channel. J Geophys Res 104:7695–7714. https://doi.org/10.1029/1998JC900038

Brzezinski MA, Washburn L (2011) Phytoplankton primary productivity in the Santa Barbara Channel: Effects of wind-driven upwelling and mesoscale eddies. J Geophys Res 116:C12013. https://doi.org/10.1029/2011JC007397

Carr SD, Capet XJ, McWilliams JC, et al (2008) The influence of diel vertical migration on zooplankton transport and recruitment in an upwelling region: estimates from a coupled behavioral-physical model. Fish Oceanogr 17:1–15. https://doi.org/10.1111/j.1365-2419.2007.00447.x

Catlett D, Siegel DA, Simons RD, et al (2021) Diagnosing seasonal to multi-decadal phytoplankton group dynamics in a highly productive coastal ecosystem. Prog Oceanogr 197:102637. https://doi.org/10.1016/j.pocean.2021.102637

Cavole L, Demko A, Diner R, et al (2016) Biological impacts of the 2013–2015 warm-water anomaly in the Northeast Pacific: Winners, losers, and the future. Oceanog 29:273–285. https://doi.org/10.5670/oceanog.2016.32

Chen G, Hou Y, Chu X (2011) Mesoscale eddies in the South China Sea: Mean properties, spatiotemporal variability, and impact on thermohaline structure. J Geophys Res 116:C06018. https://doi.org/10.1029/2010JC006716

Deutsch C, Frenzel H, McWilliams JC, et al (2021) Biogeochemical variability in the California Current System. Prog Oceanogr 196:102565. https://doi.org/10.1016/j.pocean.2021.102565

Dever EP, Hendershott MC, Winant CD (1998) Statistical aspects of surface drifter observations of circulation in the Santa Barbara Channel. J Geophys Res 103:24781–24797. https://doi.org/10.1029/98JC02403

Di Lorenzo E, Schneider N, Cobb KM, et al (2008) North Pacific Gyre Oscillation links ocean climate and ecosystem change. Geophys Res Lett 35:L08607. https://doi.org/10.1029/2007GL032838

Dong CM, Idica EY, McWilliams JC (2009) Circulation and multiple-scale variability in the Southern California Bight. Prog Oceanogr 82:168–190. https://doi.org/10.1016/j.pocean.2009.07.005

Dong CM, Lin XY, Liu Y, et al (2012) Three-dimensional oceanic eddy analysis in the Southern California Bight from a numerical product. J Geophys Res-Oceans 117:. https://doi.org/10.1029/2011jc007354

Dong CM, McWilliams JC (2007) A numerical study of island wakes in the Southern California Bight. Cont Shelf Res 27:1233–1248. https://doi.org/10.1016/j.csr.2007.01.016

Dong CM, McWilliams JC, Hall A, Hughes M (2011) Numerical simulation of a synoptic event in the Southern California Bight. J Geophys Res-Oceans 116:C05018. https://doi.org/10.1029/2010jc006578

Dorman CE, Winant CD (2000) The Structure and Variability of the Marine Atmosphere around the Santa Barbara Channel. Monthly Weather Rev 128:261. https://doi.org/10.1175/1520-0493(2000)128<0261:TSAVOT>2.0.CO;2

Dugan JE, Hubbard DM (2016) Sandy Beaches. In: Mooney HA, Zaveleta E (eds) Ecosystems of California. University of California Press, pp 389–409

Dugdale RC, Davis CO, Wilkerson FP (1997) Assessment of new production at the upwelling center at Point Conception, California, using nitrate estimated from remotely sensed sea surface temperature. J Geophys Res 102:8573–8585. https://doi.org/10.1029/96JC02136

Fennel K, Wilkin J (2009) Quantifying biological carbon export for the northwest North Atlantic continental shelves. Geophys Res Lett 36:L18605. https://doi.org/10.1029/2009GL039818

Fiedler PC, Reilly SB, Hewitt RP, et al (1998) Blue whale habitat and prey in the California Channel Islands. Deep Sea Res Part II: Top Stud Oceanogr 45:1781–1801. https://doi.org/10.1016/S0967-0645(98)80017-9

García-Reyes M, Largier JL (2012) Seasonality of coastal upwelling off central and northern California: New insights, including temporal and spatial variability. J Geophys Res 117:C03028. https://doi.org/10.1029/2011JC007629

Harms S, Winant CD (1998) Characteristic patterns of the circulation in the Santa Barbara Channel. J Geophys Res-Oceans 103:3041–3065. https://doi.org/10.1029/97jc02393

Hayward TL, Venrick EL (1998) Nearsurface pattern in the California Current: coupling between physical and biological structure. Deep Sea Res Part II: Top Stud Oceanogr 45:1617–1638. https://doi.org/10.1016/S0967-0645(98)80010-6

Henderikx Freitas F, Siegel DA, Maritorena S, Fields E (2017) Satellite assessment of particulate matter and phytoplankton variations in the Santa Barbara Channel and its surrounding waters: Role of surface waves. J Geophys Res Oceans 122:355–371. https://doi.org/10.1002/2016JC012152

Henson SA, Thomas AC (2007) Phytoplankton scales of variability in the California Current System: 1. Interannual and cross-shelf variability. J Geophys Res 112:C07017. https://doi.org/10.1029/2006JC004039

Hickey BM (1993) Chapter 2. Physical Oceanography. In: Dailey MD, Reish DJ, Anderson JW (eds) Ecology of the Southern California Bight. University of California Press, pp 19–70

Jacox MG, Bograd SJ, Hazen EL, Fiechter J (2015) Sensitivity of the California Current nutrient supply to wind, heat, and remote ocean forcing. Geophys Res Lett 42:5950–5957. https://doi.org/10.1002/2015GL065147

Jacox MG, Edwards CA, Hazen EL, Bograd SJ (2018) Coastal Upwelling Revisited: Ekman, Bakun, and Improved Upwelling Indices for the U.S. West Coast. J Geophys Res Oceans 123:7332–7350. https://doi.org/10.1029/2018JC014187

Jacox MG, Hazen EL, Bograd SJ (2016a) Optimal environmental conditions and anomalous ecosystem responses: onstraining bottom-up controls of phytoplankton biomass in the California Current System. Sci Rep 6:27612. https://doi.org/10.1038/srep27612

Jacox MG, Hazen EL, Zaba KD, et al (2016b) Impacts of the 2015–2016 El Niño on the California Current System: Early assessment and comparison to past events. Geophys Res Lett 43:7072–7080. https://doi.org/10.1002/2016GL069716

Kahru M, Kudela RM, Anderson CR, Mitchell BG (2015) Optimized merger of ocean chlorophyll algorithms of MODIS-Aqua and VIIRS. IEEE Geosci Remote Sensing Lett 12:2282–2285. https://doi.org/10.1109/LGRS.2015.2470250

Kahru M, Kudela RM, Manzano-Sarabia M, Greg Mitchell B (2012) Trends in the surface chlorophyll of the California Current: Merging data from multiple ocean color satellites. Deep Sea Res Part II: Top Stud Oceanogr 77–80:89–98. https://doi.org/10.1016/j.dsr2.2012.04.007

Kilpatrick T, Xie S, Miller AJ, Schneider N (2018) Satellite observations of enhanced chlorophyll variability in the Southern California Bight. J Geophys Res: Oceans 123:7550–7563. https://doi.org/10.1029/2018JC014248

Krause JW, Brzezinski MA, Siegel DA, Thunell RC (2013) Biogenic silica standing stock and export in the Santa Barbara Channel ecosystem. J Geophys Res Oceans 118:736–749. https://doi.org/10.1029/2012JC008070

Kudela RM, Chavez FP (2002) Multi-platform remote sensing of new production in central California during the 1997–1998 El Niño. Progr Oceanogr 54:233–249. https://doi.org/10.1016/S0079-6611(02)00051-4

Lachkar Z, Gruber N (2011) What controls biological production in coastal upwelling systems? Insights from a comparative modeling study. Biogeosci 8:2961–2976. https://doi.org/10.5194/bg-8-2961-2011

Legaard KR, Thomas AC (2006) Spatial patterns in seasonal and interannual variability of chlorophyll and sea surface temperature in the California Current. J Geophys Res 111:C06032. https://doi.org/10.1029/2005JC003282

Levin LA, Liu K-K, Emeis K-C, et al (2015) Comparative biogeochemistry–ecosystem–human interactions on dynamic continental margins. J Mar Syst 141:3–17. https://doi.org/10.1016/j.jmarsys.2014.04.016

Liu Y, Dong C, Guan Y, et al (2012) Eddy analysis in the subtropical zonal band of the North Pacific Ocean. Deep Sea Res Part I:Oceanogr Res Papers 68:54–67. https://doi.org/10.1016/j.dsr.2012.06.001

Lynn KJ, Baumgaktnek T, Garcia J, et al (1998) The state of the California Current, 1997-1998: Transistion to El Nino Conditions. Calif Coop Fish Invest Rep 39:25–49

Mantyla AW, Venrick EL, Hayward TL (1995) Primary productions and chlorophyll relationships, derived from ten years of CalCOFI measurements. Calif Coop Fish Invest Rep 36:159–166

Matson PG, Washburn L, Fields EA, et al (2019) Formation, development, and propagation of a rare coastal Coccolithophore bloom. J Geophys Res: Oceans 124:3298–3316. https://doi.org/10.1029/2019JC015072

McClatchie S, Jacox MG, Ohman MD, et al (2016) State of the California Current 2015–16: Comparisons with the 1997–98 El Nino. Calif Coop Fish Invest Rep 57:5–61

McGillicuddy DJ (2016) Mechanisms of physical-biological-biogeochemical interaction at the oceanic mesoscale. Annu Rev Mar Sci 8:125–159. https://doi.org/10.1146/annurev-marine-010814-015606

McPhee-Shaw EE, Siegel DA, Washburn L, et al (2007) Mechanisms for nutrient delivery to the inner shelf: Observations from the Santa Barbara Channel. Limnol Oceanogr 52:1748–1766. https://doi.org/10.4319/lo.2007.52.5.1748

Melton C, Washburn L, Gotschalk C (2009) Wind relaxations and poleward flow events in a coastal upwelling system on the central California coast. J Geophys Res 114:C11016. https://doi.org/10.1029/2009JC005397

Messié M, Chavez FP (2015) Seasonal regulation of primary production in eastern boundary upwelling systems. Progr Oceanogr 134:1–18. https://doi.org/10.1016/j.pocean.2014.10.011

Michaud KM, Reed DC, Miller RJ (2022) The Blob marine heatwave transforms California kelp forest ecosystems. Commun Biol 5:1143. https://doi.org/10.1038/s42003-022-04107-z

Miller RJ, Reed DC, Brzezinski MA (2011) Partitioning of primary production among giant kelp (*Macrocystis pyrifera*), understory macroalgae, and phytoplankton on a temperate reef. Limnol Oceanogr 56:119–132. https://doi.org/10.4319/lo.2011.56.1.0119

Mitarai S, Siegel DA, Watson JR, et al (2009) Quantifying connectivity in the coastal ocean with application to the Southern California Bight. J Geophys Res-Oceans 114:C10026. https://doi.org/10.1029/2008JC005166

Nencioli F, Dong C, Dickey T, et al (2010) A vector geometry–based eddy detection algorithm and its application to a high-resolution numerical model product and high-frequency radar surface velocities in the Southern California Bight. J Atmos Ocean Technol 27:564–579. https://doi.org/10.1175/2009JTECHO725.1

Nishimoto M, Washburn L (2002) Patterns of coastal eddy circulation and abundance of pelagic juvenile fish in the Santa Barbara Channel, California, USA. Mar Ecol Prog Ser 241:183–199. https://doi.org/10.3354/meps241183

Oey L-Y, Wang D-P, Hayward T, et al (2001) “Upwelling” and “cyclonic” regimes of the near-surface circulation in the Santa Barbara Channel. J Geophys Res 106:9213–9222. https://doi.org/10.1029/1999JC000129

Oey L-Y, Winant C, Dever E, et al (2004) A model of the near-surface circulation of the Santa Barbara Channel: Comparison with observations and dynamical interpretations. J Phys Oceanogr 34:23–43. https://doi.org/10.1175/1520-0485(2004)034<0023:AMOTNC>2.0.CO;2

Ohlmann JC, Mitarai S (2010) Lagrangian assessment of simulated surface current dispersion in the coastal ocean. Geophys Res Lett 37:L17602. https://doi.org/10.1029/2010GL044436

Omand MM, Feddersen F, Guza RT, Franks PJS (2012) Episodic vertical nutrient fluxes and nearshore phytoplankton blooms in Southern California. Limnol Oceanogr 57:1673–1688. https://doi.org/10.4319/lo.2012.57.6.1673

Otero M, Siegel D (2004) Spatial and temporal characteristics of sediment plumes and phytoplankton blooms in the Santa Barbara Channel. Deep Sea Res Part II: Top Stud Oceanogr 51:1129–1149. https://doi.org/10.1016/S0967-0645(04)00104-3

Palacios DM, Hazen EL, Schroeder ID, Bograd SJ (2013) Modeling the temperature-nitrate relationship in the coastal upwelling domain of the California Current: Modeling the T-N Relationship. J Geophys Res Oceans 118:3223–3239. https://doi.org/10.1002/jgrc.20216

Quilfen Y, Shutler J, Piolle J-F, Autret E (2021) Recent trends in the wind-driven California current upwelling system. Remote Sens Environ 261:112486. https://doi.org/10.1016/j.rse.2021.112486

Santora JA, Sydeman WJ, Schroeder ID, et al (2017) Persistence of trophic hotspots and relation to human impacts within an upwelling marine ecosystem. Ecol Appl 27:560–574. https://doi.org/10.1002/eap.1466

Santoro AE, Nidzieko NJ, Dijken GL van, et al (2010) Contrasting spring and summer phytoplankton dynamics in the nearshore Southern California Bight. Limnol Oceanogr 55:264–278. https://doi.org/10.4319/lo.2010.55.1.0264

Schwing FB, Moore CS, Ralston S, Sakuma KM (2000) Record coastal upwelling in the California Current. Calif Coop Fish Invest Rep 41:148–160

Shchepetkin AF, McWilliams JC (2005) The regional oceanic modeling system (ROMS): a split-explicit, free-surface, topography-following-coordinate oceanic model. Ocean Model 9:347–404. https://doi.org/10.1016/j.ocemod.2004.08.002

Shipe RF, Brzezinski MA (2001) A time series study of silica production and flux in an eastern boundary region: Santa Barbara Basin, California. Global Biogeochem Cycles 15:517–531. https://doi.org/10.1029/2000GB001297

Shipe RF, Passow U, Brzezinski MA, et al (2002) Effects of the 1997–98 El Niño on seasonal variations in suspended and sinking particles in the Santa Barbara basin. Progr Oceanogr 54:105–127. https://doi.org/10.1016/S0079-6611(02)00045-9

Siegel DA, Behrenfeld MJ, Maritorena S, et al (2013) Regional to global assessments of phytoplankton dynamics from the SeaWiFS mission. Remote Sensing of Environment 135:77–91. https://doi.org/10.1016/j.rse.2013.03.025

Simons RD, Nishimoto MM, Washburn L, et al (2015) Linking kinematic characteristics and high concentrations of small pelagic fish in a coastal mesoscale eddy. Deep Sea Res Part I: Oceanogr Res Papers 100:34–47. https://doi.org/10.1016/j.dsr.2015.02.002

Snyder JN, Bell TW, Siegel DA, et al (2020) Sea surface temperature imagery elucidates spatiotemporal nutrient patterns for offshore kelp aquaculture siting in the Southern California Bight. Front Mar Sci 7:22. https://doi.org/10.3389/fmars.2020.00022

Stone HB, Banas NS, MacCready P, et al (2020) Linking chlorophyll concentration and wind patterns using satellite data in the Central and Northern California Current System. Front Mar Sci 7:551562. https://doi.org/10.3389/fmars.2020.551562

Strub PT, James C (2000) Altimeter-derived variability of surface velocities in the California Current System: 2. Seasonal circulation and eddy statistics. Deep Sea Res Part II: Top Stud Oceanogr 47:831–870. https://doi.org/10.1016/S0967-0645(99)00129-0

Sydeman WJ, García-Reyes M, Schoeman DS, et al (2014) Climate change and wind intensification in coastal upwelling ecosystems. Science 345:77–80. https://doi.org/10.1126/science.1251635

Thomson RE, Emery WJ (2014) The Spatial Analyses of Data Fields. In: Data Analysis Methods in Physical Oceanography. Elsevier, pp 313–424

Thunell R, Benitez-Nelson C, Varela R, et al (2007) Particulate organic carbon fluxes along upwelling-dominated continental margins: Rates and mechanisms. Global Biogeochem Cycles 21:GB1022. https://doi.org/10.1029/2006GB002793

Venrick EL (1998) The phytoplankton of the Santa Barbara Basin: Patterns of chlorophyll and species structure and their relationships with those of surrounding stations. Calif Coop Fish Invest Rep 39:124–132

Wang D, Gouhier TC, Menge BA, Ganguly AR (2015) Intensification and spatial homogenization of coastal upwelling under climate change. Nature 518:390–394. https://doi.org/10.1038/nature14235

Wang X, Du Y, Zhang Y, et al (2021) Influence of two eddy pairs on high-salinity water intrusion in the Northern South China Sea during fall-winter 2015/2016. J Geophys Res: Oceans 126:e2020JC016733. https://doi.org/10.1029/2020JC016733

Washburn L, McPhee-Shaw E (2013) Coastal Transport Processes Affecting Inner-Shelf Ecosystems in the California Current System. oceanog 26:34–43. https://doi.org/10.5670/oceanog.2013.43

Wilkerson FP, Lassiter AM, Dugdale RC, et al (2006) The phytoplankton bloom response to wind events and upwelled nutrients during the CoOP WEST study. Deep Sea Res Part II: Top Stud Oceanogr 53:3023–3048. https://doi.org/10.1016/j.dsr2.2006.07.007

Winant CD, Dever EP, Hendershott MC (2003) Characteristic patterns of shelf circulation at the boundary between central and southern California. J Geophys Res 108:3021. https://doi.org/10.1029/2001JC001302

Winant CD, Dorman CE (1997) Seasonal patterns of surface wind stress and heat flux over the Southern California Bight. J Geophys Res 102:5641–5653. https://doi.org/10.1029/96JC02801

Supplementary Information

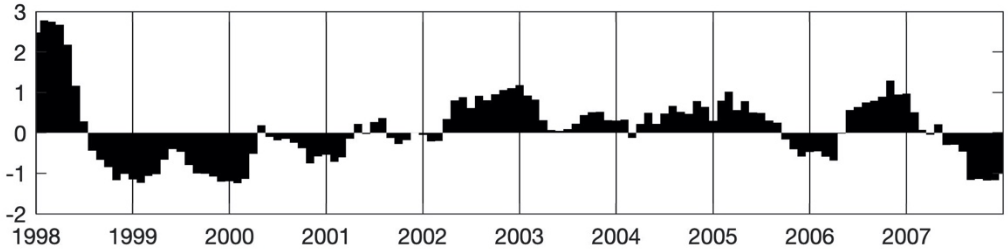

Figure S1: MEI (pls.noaa.gov/enso/mei, Wolter and Timlin 1993, 1998)

<u>Comparison of temperature from ROMS to field observations during the SUP</u>

The accuracy of the temperature predictions from ROMS in the SBC surface layer is important for this study as N_{max}, representing nutrient availability, is estimated from temperature (see Section 2.4). To determine the accuracy of the temperature during the SUP, field observations of temperature at 8 stations in the SBC (Figure S2) are compared to temperature predictions from ROMS. The stations are located along the SBC coastline; four (ALE, NAP, MKO, and CAR) on the mainland, three (PEL, SCP, and TRL) on the north coast of Santa Cruz Island, and one on the coast of Anacapa Island (ANS). At these stations, continuously logged temperature data at 14 m depth starting from 2000-2004 through 2007 is available from the Santa Barbara Coastal Long-Term Ecological Research site (sbclter.msi.ucsb.edu, Washburn et al. 2022).

For each year from 2000-2007, the root-mean-square error (RMSE) between the temperature from ROMS and the field station during the SUP is calculated and presented in Tables S1. The model and field temperature show good agreement with RMSE ranging from 0.6 to 1.6°C per year when averaged over all stations. The year that shows the best agreement is the 2001 SUP with a RMSE ranging from 0.6 to 0.8°C per station. ROMS and field temperature data for the 2001 SUP is shown in Figure 3S for six stations.

Station	2000	2001	2002	2003	2004	2005	2006	2007
ALE	1.2	0.7	1.1	1.6	0.9	1.4	1.2	1.0
NAP	NA	0.6	1.1	1.3	1.4	1.5	1.2	1.4
MKO	NA	NA	NA	2.8	2.3	1.1	2.1	1.9
CAR	NA	0.8	1.0	2.3	2.3	1.2	1.9	1.8
PEL	1.4	0.5	1.1	1.0	1.1	1.3	1.6	1.7
SCP	1.3	0.5	1.3	1.0	1.0	1.4	1.5	1.6
TRL	1.2	0.6	0.8	1.0	0.8	1.8	1.2	1.5
ANS	NA	NA	NA	1.6	1.6	1.5	1.3	1.6
Mean	1.3	0.6	1.1	1.6	1.4	1.4	1.5	1.6

Table S1: Temperature RMSE (°C) between ROMS and field station data

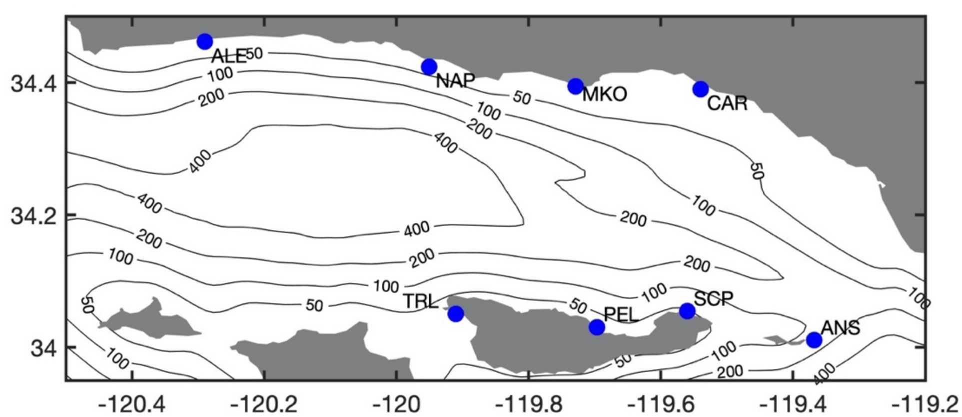

Figure S2: Santa Barbara Channel with bathymetry (meters) and temperature stations (blue circles).

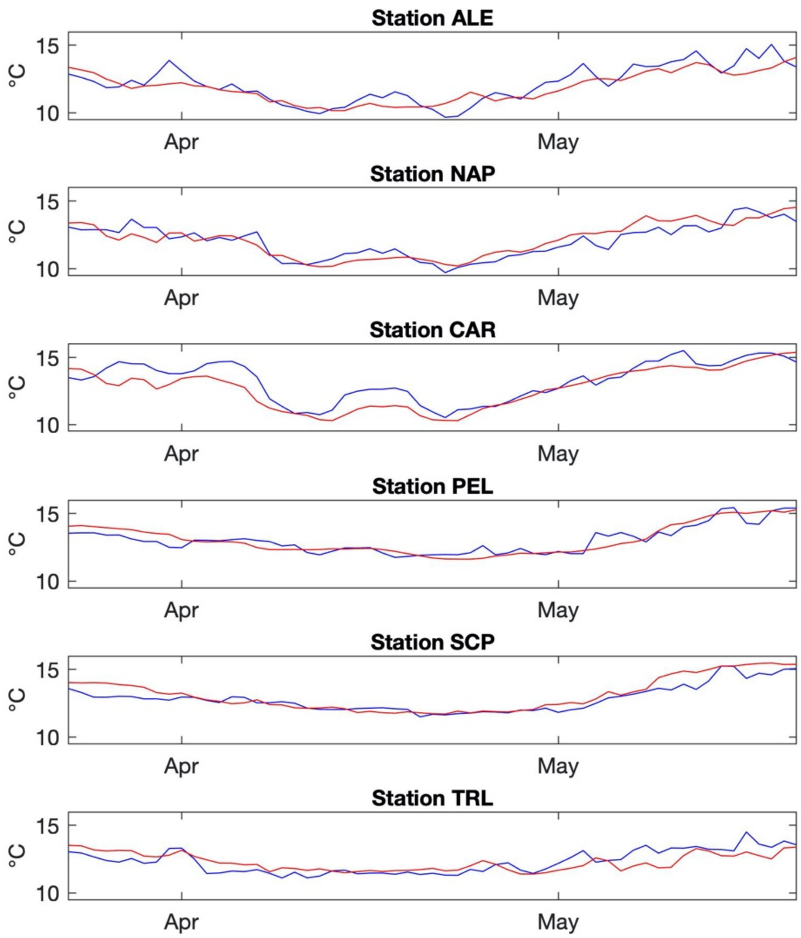

Figure S3: Temperature data for the 2001 SUP. The blue line is the field data, and the red line is the ROMS data.

<u>References</u>

Washburn L, Gotschalk C, Salazar D (2022) SBC LTER: Ocean: Currents and Biogeochemistry: Moored CTD and ADCP data from Alegria Reef Mooring (ALE), ongoing since 1999

Wolter K, Timlin MS (1993) Monitoring ENSO in COADS with a Seasonally Adjusted Principal Component Index. Proceedings of the 17th Climate Diagnostics Workshop, Norman, 18-23 October 1992 52–57

Wolter K, Timlin MS (1998) Measuring the strength of ENSO events: How does 1997/98 rank? Weather 53:315–324. https://doi.org/10.1002/j.1477-8696.1998.tb06408.x